iScience

CellPress

Article

Fundamental Characteristics of Single-Cell Aging in Diploid Yeast

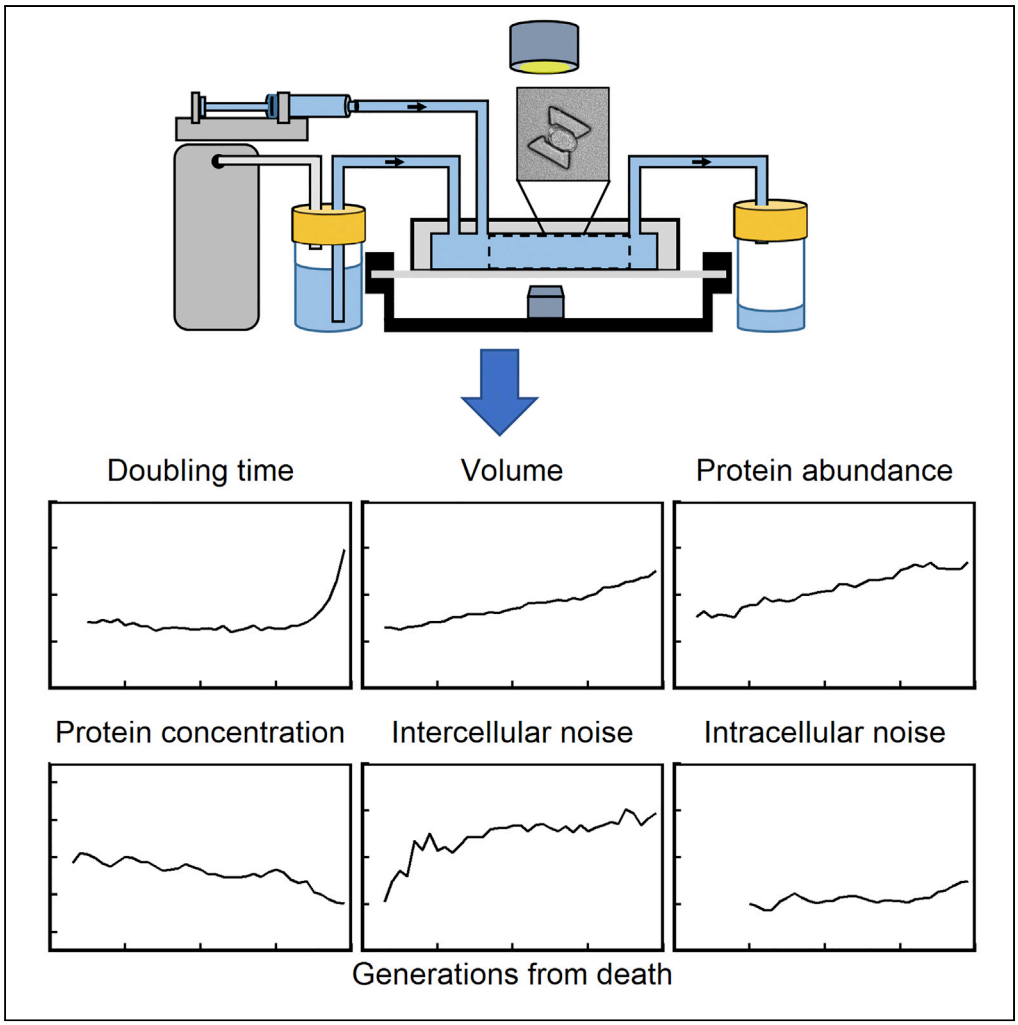

Ethan A. Sarnoski, Ruijie Song, Ege Ertekin, Noelle Koonce, Murat Acar

murat.acar@yale.edu

HIGHLIGHTS

A microfluidic device facilitates longitudinal observation of aging diploid yeast

Proteins with short versus long half-lives exhibit distinct dynamics as cells age

Intercellular gene expression noise increases during replicative aging

Unlike haploid yeast, intracellular noise is unchanged during aging in diploid yeast

Sarnoski et al., iScience 7, 96–109
September 28, 2018
https://doi.org/10.1016/j.isci.2018.08.011

iScience

CellPress

Article

Fundamental Characteristics of Single-Cell Aging in Diploid Yeast

Ethan A. Sarnoski,[1,2] Ruijie Song,[2,3] Ege Ertekin,[1,2] Noelle Koonce,[1,2] and Murat Acar[1,2,3,4,5,*]

SUMMARY

Single-cell-level experimentation can elucidate key biological insights about cellular aging that are masked in population-level studies. However, the extensive time requirement of tracking single cells has historically prevented their long-term longitudinal observation. Using a microfluidic device that automates microscopic monitoring of diploid *Saccharomyces cerevisiae* cells throughout their replicative lifespan, here we report the fundamental characteristics of single-cell aging for diploid yeast. We find that proteins with short versus long half-lives exhibit distinct dynamics as cells age and that the intercellular gene expression noise increases during aging, whereas the intracellular noise stays unchanged. A stochastic model provides quantitative mechanistic insights into the observed noise dynamics and sheds light on the age-dependent intracellular noise differences between diploid and haploid yeast. Our work elucidates how a set of canonical phenotypes dynamically change while the host cells are aging in real time, providing essential insights for a comprehensive understanding on and control of lifespan at the single-cell level.

INTRODUCTION

The replicative lifespan (RLS) of *Saccharomyces cerevisiae* is defined as the number of daughters a mother cell produces before its death. Studies of yeast RLS have played a critical role in elucidating evolutionarily conserved aging pathways (Wasko and Kaeberlein, 2014), including dietary restriction and the mTOR pathway. An important benefit of yeast RLS as an aging model is its rapidity: most cells die within several days of birth. Traditional methods for measuring RLS require manual removal and counting of daughter cells (Steffen et al., 2009). This limitation not only constrains throughput but also requires laboratories to refrigerate the cells overnight to slow division as researchers sleep. Together, these constraints prevent the acquisition of large datasets and compromise reproducibility.

Our laboratory and others have developed devices that permit automated, full-lifespan monitoring of RLS (Chen et al., 2017; Liu et al., 2015). These devices increase throughput and maintain a constant temperature, but they have been designed exclusively for the haploid form of *S. cerevisiae*. Yeast exist in both haploid and diploid states (Herskowitz, 1988), with significant differences between the two in terms of cell size and morphology: spherical haploids occupy approximately half of the volume occupied by elliptical diploids. Due to these differences, the microfluidic device (termed the Replicator) that we have developed for trapping and tracking haploid yeast cells during their aging cannot be used for diploid cells. A device that works for diploid yeast cells needs to have an elliptical cell-trapping unit that is optimized in size so that the inner area of the unit is just the "right" size; this optimization is necessary as smaller trap sizes would not allow a newborn cell to enter the trapping unit, whereas larger sizes would not be able to keep the cell trapped during the multi-day experiments.

Haploid and diploid yeast are suited to particular research purposes. Haploid *S. cerevisiae* benefit from facile genetic manipulation and a shorter RLS, making them ideal for screening studies. The longer lived diploid *S. cerevisiae*, however, are uniquely compatible with experiments that require a chromosomal complement ≥ 2, such as those investigating loss of heterozygosity (LOH) (McMurray and Gottschling, 2003) or differentiating intrinsic and extrinsic noise (Swain et al., 2002). Furthermore, wild yeasts exist primarily in the diploid state, and studies in diploids may thus be preferable for understanding the evolutionary roots of aging. The quantification of intrinsic and extrinsic noise requires a double reporter system with each reporter integrated at identical loci (Elowitz et al., 2002; Raser and O'Shea, 2004). Intrinsic noise excludes variations due to changes in the intracellular environment that affects all genes in the same cell, which is not possible to measure without a double-reporter system integrated at two identical loci in diploid cells.

[1]Department of Molecular Cellular and Developmental Biology, Yale University, 219 Prospect Street, New Haven, CT 06511, USA

[2]Systems Biology Institute, Yale University, 850 West Campus Drive, West Haven, CT 06516, USA

[3]Interdepartmental Program in Computational Biology and Bioinformatics, Yale University, 300 George Street, Suite 501, New Haven, CT 06511, USA

[4]Department of Physics, Yale University, 217 Prospect Street, New Haven, CT 06511, USA

[5]Lead Contact

*Correspondence: murat.acar@yale.edu

https://doi.org/10.1016/j.isci.2018.08.011

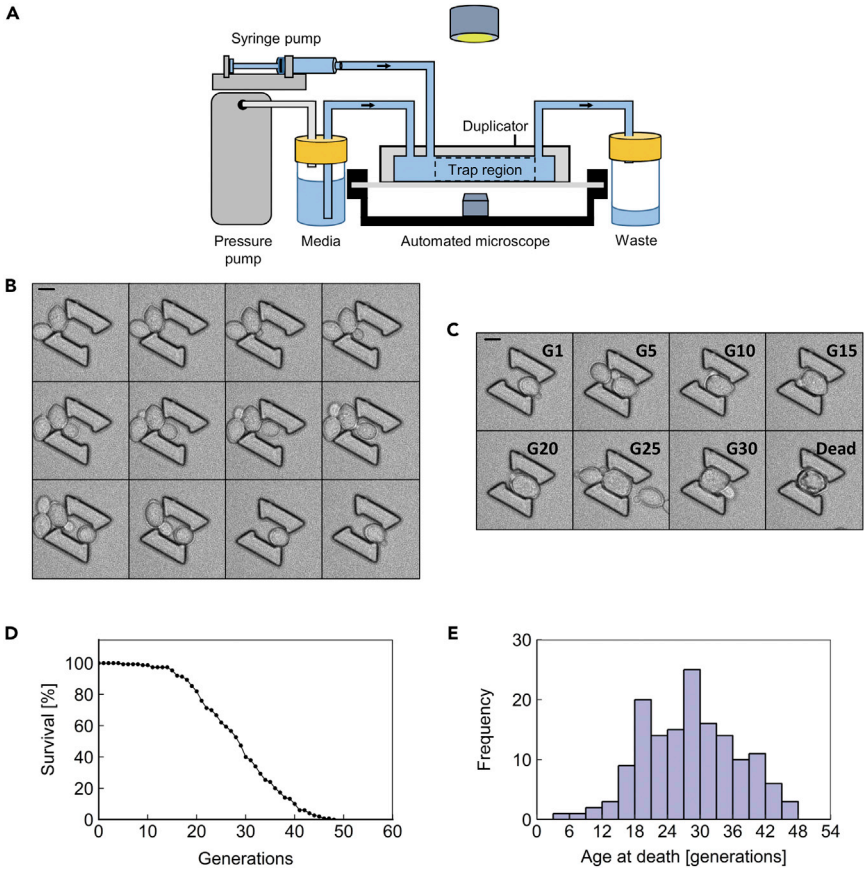

Figure 1. The Duplicator

(A) A schematic representation of the Duplicator assembly. Media is supplied via a pressure-driven pump, whereas cells are loaded using a syringe pump. Liquid flows through the Duplicator apparatus into a collection tube. Images are collected using an automated microscope.

(B) Representative time-lapse images at 10-min intervals for a single cell budding into a Duplicator trap. Scale bar, 4.95 μm.

(C) Representative time-lapse images for a single cell at specified generations (G) throughout its lifespan. This cell lived to 33 generations. Scale bar, 4.95 μm.

(D) A viability curve composed of 150 cells from 3 replicate experiments performed in the Duplicator for the BY4743 wild-type background.

(E) The histogram version of the RLS data plotted in (D).

See also Figure S1 and Table S1.

RESULTS

A Microfluidic Device to Measure Single-Cell Aging Phenotypes from Diploid Yeast Cells

We developed a microfluidic device that enables an automated microscope to image hundreds of diploid *S. cerevisiae* cells throughout their full RLS (Figures 1A–1E, Table S1, Video S1). We based this device, termed the Duplicator, on our previously published Replicator (Liu et al., 2015) device designed for tracking haploid yeast cells throughout their lifespan.

To evaluate the performance of the microfluidic device, we ran 3 independent Duplicator experiments in which we took time-lapse images of wild-type yeast cells at 10-min intervals for 120 hr, a duration that was sufficient to follow each diploid cell from birth to death. For each experiment, we assessed the lifespan of 50 wild-type cells (Figures 1D, 1E, and S1). The mean lifespan for cells combined from all 3 experiments was 29.0 $\pm$ 0.7 generations, with mean values for each individual experiment falling within 5% of the overall mean value (Figure S1A and Table S1). This RLS approximates published values for the diploid BY4743 strain used in our experiments (Delaney et al., 2013; Yang et al., 2011) and exceeds the lifespan of the haploid BY4741 strain (Liu et al., 2015), as expected.

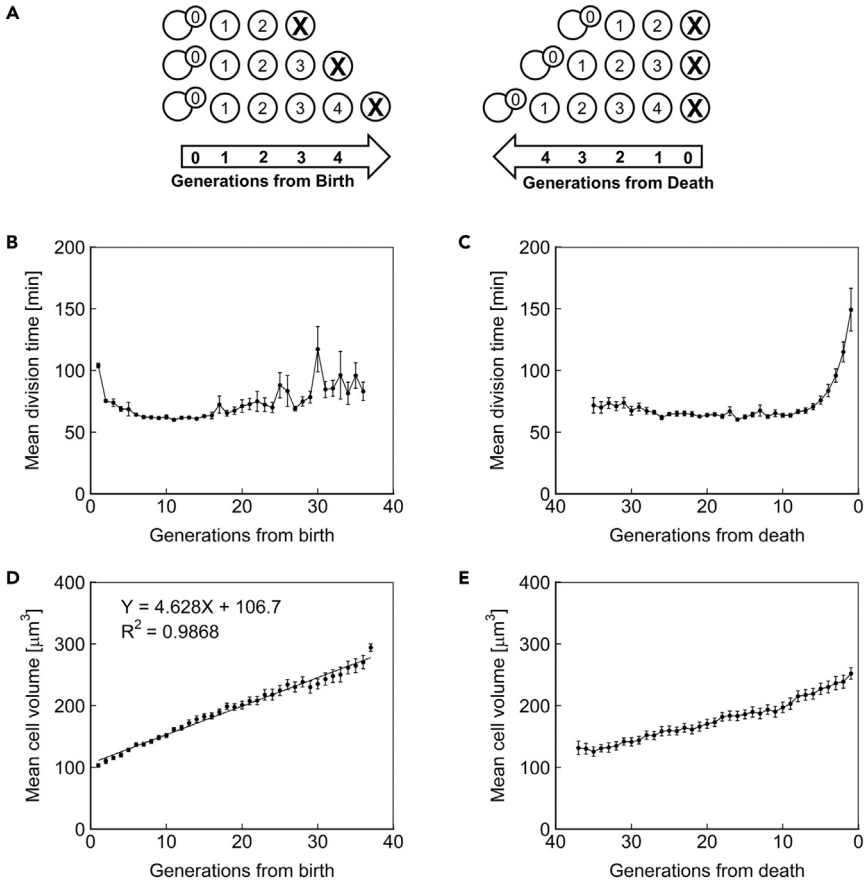

Figure 2. Fundamental Characteristics of Aging Cells

(A) A schematic demonstrating the principle of cell alignment at birth (left) or to death (right). Individual cells' generational age is displayed within their representation.

(B) Mean division time as a function of age, with cells aligned to birth.

(C) Mean division time as a function of age, with cells aligned at death.

(D) Mean volume of cells as a function of age, with cells aligned to birth. The best-fit line from linear regression is shown.

(E) Mean volume of cells as a function of age, with cells aligned at death. N = 50 cells for all subfigures, with data points where less than 10 cells remained alive omitted. Error bars are SEM.

Characterization of Age-Related Changes in Cell-Cycle Durations in Diploid Yeast Cells

We used the Duplicator platform to investigate the fundamental characteristics of aging diploid yeast. The dynamics of an aging cell can be probed from either a birth-centric or a death-centric perspective; therefore, we aligned single-cell measurements either to the number of generations that had elapsed since the birth of the cell or to the number of generations that remained until the death of the cell (Figure 2A). Aligning measurements to birth relates trends to a cell's distance from the newborn state, whereas alignment to cell death highlights the phenotypes that immediately precede death.

We first sought to delineate age-related changes in the cell cycle. Previous reports have demonstrated that the first generation of a haploid cell's life is substantially longer than subsequent generations (Ferrezuelo et al., 2012). We observed the same phenotype for diploid cells (Figure 2B). We also observed that cell-cycle duration increases in the last few generations of life (Figure 2C), consistent with our prior observations in haploids (Liu and Acar, 2018; Liu et al., 2017). However, until the last few generations of life, diploid yeast cells displayed steady cell-cycle durations (Figure 2C), whereas haploid yeast had shown increasing cell-cycle durations across their full lifespan (Liu and Acar, 2018). Assuming that longer cell-cycle durations are reflections of the extra time needed for the repair of aging-related damage to cellular components, the difference between diploid and haploid cells in terms of cell-cycle duration dynamics suggests that

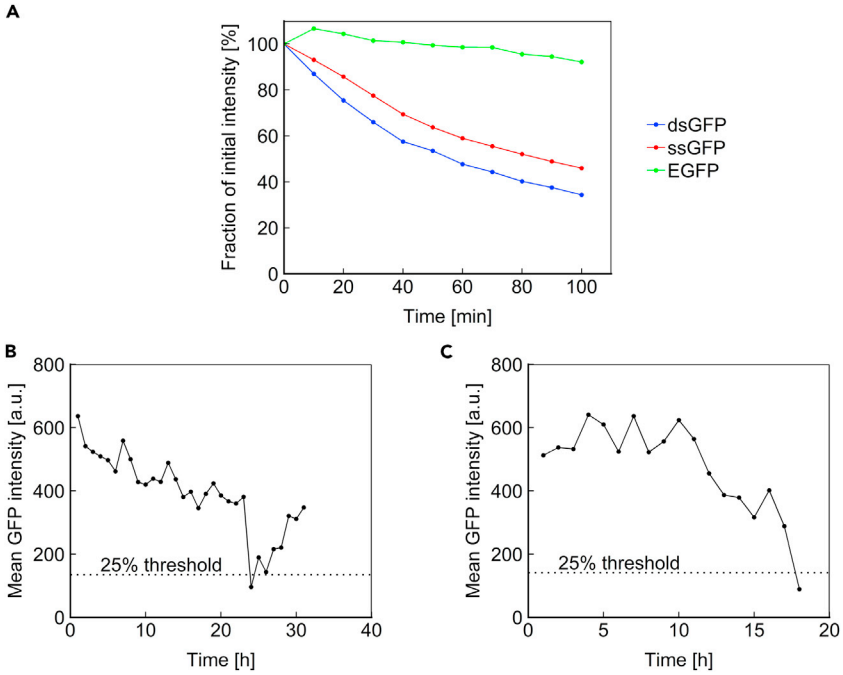

Figure 3. Loss of Heterozygosity Is a Rare Event in the Yeast Lifespan

(A) Fluorescence intensity versus time after blocking translation with cycloheximide for cells expressing EGFP, destabilized GFP (dsGFP), or semi-stable GFP (ssGFP).

(B) ssGFP intensity over time for a representative cell for which fluorescence intensity fell below the 25% threshold, defining the first criteria for LOH.

(C) ssGFP intensity over time for the only cell that exhibited a decline below the 25% threshold and did not subsequently recover.

diploid cells have a greater damage tolerance compared with haploids due to the ploidy-based greater abundance of all cellular components.

Cell Volume Increases Linearly with Replicative Age in Diploid Yeast

We next aimed to measure the cell volume dynamics throughout the lifespan. With each generation, yeast cells grow in volume. This phenotype has been suggested to play a role in mortality, based on the observation that short-lived mutant strains often display the same terminal volume as their wild-type counterparts (Yang et al., 2011; Zadrag-Tecza et al., 2009). We approximated the volume of aging diploid *S. cerevisiae* by assuming an ellipsoid shape and solving for volume with measured values for area and perimeter. We observed an initial volume of 103 μm^3, a linear growth of 4.6 μm^3/generation, and a terminal volume of 294 μm^3 (Figure 2D). A similar trend was observed when cells were aligned to death (Figure 2E). Interestingly, the 294 μm^3 terminal volume of the diploid BY4743 exceeded the ~190 μm^3 observed for haploid BY4741 (Zadrag-Tecza et al., 2009), indicating that either volume does not limit the lifespan or that ploidy determines resistance to the associated cause of death.

Directly Measuring Loss of Heterozygosity in Aging Mother Cells

Using population-level and indirect assays, LOH has previously been associated with aging in multiple model organisms (McMurray and Gottschling, 2003; Siudeja et al., 2015; Wiktor-Brown et al., 2006). We sought to directly observe LOH in a longitudinal fashion for single mother cells over their entire lifespan. For this, we chose to use a constitutively expressed fluorescent reporter cassette whose absence would indicate LOH. EGFP and other standard fluorescent proteins have very long lifetimes, with half-lives of multiple days (Natarajan et al., 1998). To increase temporal resolution to identify an LOH event, we performed experiments using a short-lived fluorescent protein. Destabilized GFP (dsGFP), which was generated by fusing EGFP to a degradation sequence from the Cln2 protein (Mateus and Avery, 2000), displayed a half-life of ~50 min (Figure 3A). Although such a short half-life would enable near-immediate detection

of an LOH event, the high degradation rate leads to low steady-state expression of this protein, necessitating bright fluorescent exposure for its measurement, which can be harmful to cells. Therefore, we constructed a semi-stable GFP (ssGFP) by removing part of the destabilization tag from dsGFP (Salama et al., 1994). The resulting protein had a half-life of 84 min (Figure 3A), striking a balance between fluorescence intensity and temporal resolution of LOH detection. Using the half-life measurement method we applied in this study, the median half-life of yeast proteins was shown to be ~43 min (without dilution by cell division) (Belle et al., 2006). The ssGFP reporter we use in this study exhibits a half-life comparable to many native yeast proteins, whereas EGFP exhibits a half-life on the order of 20+ hours.

Using a colony-based assay, a previous study estimated that the rate of LOH at the unstable *SAM2* locus is at ~2% of cell divisions in aged yeast (McMurray and Gottschling, 2003). As diploid mother cells aged, an age-induced switch to a hyper-recombinational state was reported, leading to ~100-fold increase in LOH, based on assessing the color of the colonies formed from the daughter cells dissected from the aging mother cells. The definition of an "aged" mother cell was based on the first time one of its daughters displayed an LOH event, instead of using a specific generation-number-based cutoff. Here we sought to measure the rate of LOH directly in mother cells aging in real time. For this, we integrated ssGFP driven by the constitutive *TEF1* promoter (P_{TEF1}) at one copy of the *SAM2* locus in a diploid yeast strain. Using the Dupli-cator, we imaged ssGFP intensity at hourly intervals for the duration of the cells' lifespan. Measurements of age-specific ssGFP intensity for 96 mother cells from 20 imaging locations were included in our analyses. We determined that 3 criteria should be met to confirm an LOH event. (1) The ssGFP intensity should drop to <25% of a healthy cell's level, which should occur ~3 hr after the LOH event based on the half-life of ssGFP; 6 of 96 cells met this criterion (Figure 3B). (2) The ssGFP intensity should not subsequently increase, as this phenotype is not consistent with LOH. Only 1 of 6 cells that met the first criterion did not exhibit a subsequent increase in ssGFP intensity (Figure 3C). (3) The cell should live for at least 3 additional generations, such that we can confirm that the ssGFP has not been temporarily depressed. The cell that passed the second criterion crossed beyond the 25% threshold in only its final measurement. Therefore, none of the tracked cells satisfied the criteria set for observing an LOH event. Counting the total number of cell divisions experienced by the 96 cells tracked, we saw that the cells completed 2,799 divisions across their full lifespans. We report 0% LOH rate (95% confidence interval [CI], 0%–0.13%) at the *SAM2* locus based on our direct measurements in aging mother cells, whereas if we counted the experience of the one cell that crossed beyond the 25% threshold in its final measurement as an LOH event, then we would have reported ~0.04% (=1/2,799; 95% CI, 0%–0.2%) as the single-cell-level LOH rate per cell division. Together, our findings suggest that diploid mother cells experience rare LOH events, if any, across the whole genome.

Aging Yeast Exhibit Distinct Dynamics of Protein Concentration and Abundance

Most studies of gene expression dynamics are performed using stable fluorescent proteins such as EGFP, for which half-life is substantially greater than that of a typical natural protein (Belle et al., 2006). ssGFP's half-life of 84 min approaches the median half-life of *S. cerevisiae* proteins of ~43 min measured by a similar technique (Belle et al., 2006). We therefore sought to characterize the expression dynamics of ssGFP on a single-cell level throughout the aging process of diploid yeast as an accurate marker of gene expression.

The protein amount in a cell can be conveyed in terms of concentration or total abundance. These 2 variables are closely related through cell volume but have distinct biological meanings. We defined ssGFP concentration as the mean pixel intensity of the cell and ssGFP abundance as the mean pixel intensity multiplied by cell volume. ssGFP concentration declined ~20% over the lifespan (Figure 4A) and exhibited a more rapid decline immediately before death (Figure 4B). Conversely, we observed an ~50%–100% increase in ssGFP abundance across the lifespan (Figures 4C and 4D). We note that due to changes in volume as cells age (Figures 2D and 2E), it is impossible that protein concentration and abundance both remain constant during aging.

Characterization of Gene Expression Variability during Aging in Diploid Yeast

In addition to mean values, protein expression can be characterized in terms of variability, either longitudinally within a single cell or between cells. We define intercellular variability as the SD(σ) divided by the mean (μ) for the concentrations of all cells within a population. Intracellular variability is defined as σ/μ for measurements of a given cell across a set number of generations, and is expressed as the average intracellular variability for the population of cells of a given age. Therefore, intercellular variability is a measure

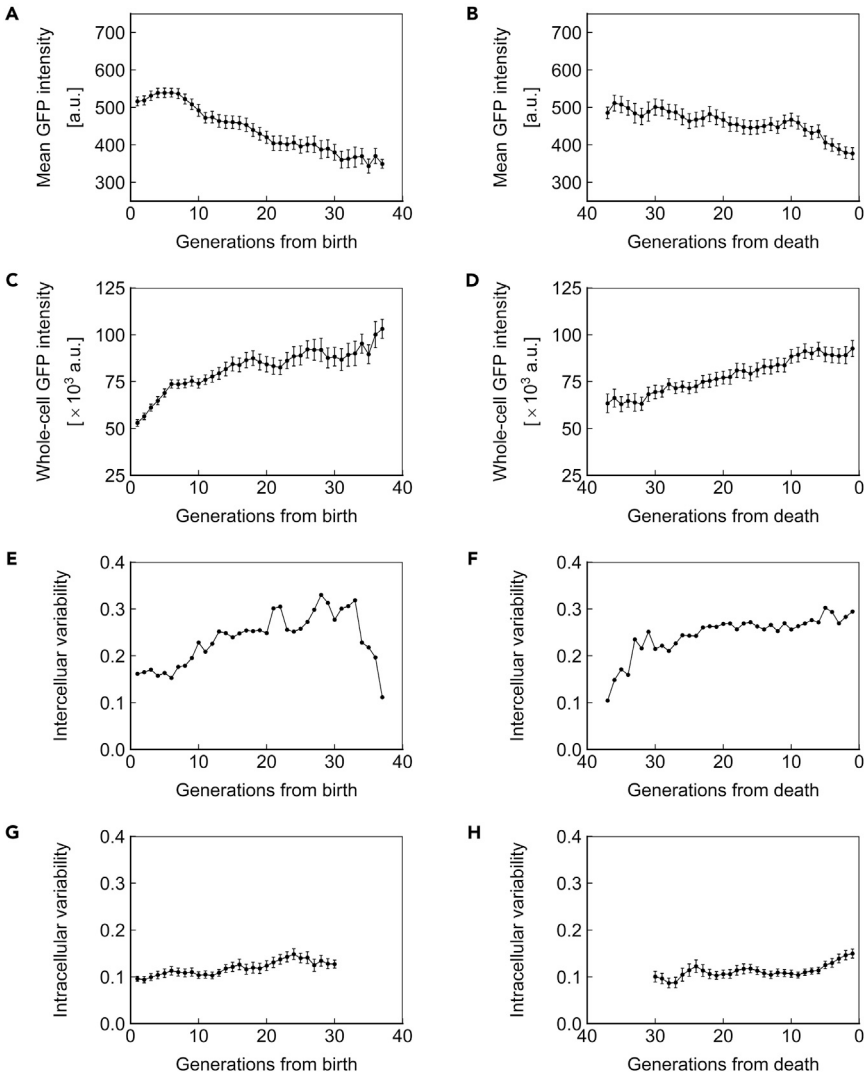

Figure 4. Short-Lived Reporter Dynamics in Aging Cells

(A and B) Mean ssGFP intensity, a measure of protein concentration, over generations for cells aligned to birth (A) or death (B).

(C and D) Whole-cell ssGFP intensity, a measure of protein abundance, over generations for cells aligned to birth (C) or death (D).

(E and F) Intercellular variability, defined as the SD divided by the mean for mean ssGFP intensity across measurements of all cells in the population at each generation. In (E), cells are aligned at birth, and in (F), cells are aligned at death.

(G and H) Mean intracellular variability, defined as the SD/mean of mean ssGFP intensity for 8 contiguous generations, over generations for cells aligned to birth (G) or death (H). All data represent measurements from a single experiment with ssGFP integrated in a heterozygous fashion at the *SAM2* locus under the P_{TEF1} promoter. N = 50 cells for all subfigures, with data points where less than 10 cells remained alive omitted. Error bars are SEM.

See also Figures S2 and S7, and Tables S2–S4.

of the population-level heterogeneity, whereas intracellular variability is a measure of a single cell's inconsistency in expression level.

Cells in a population are expected to be the most similar, and thus exhibit the least intercellular variability, at the point they are aligned to a common trait. Indeed, when cells were aligned at birth, we observed relatively low intercellular variability (coefficient of variation [CV]: ~0.15) among the young cells (Figure 4E). However, when cells were aligned on the basis of death, we saw high intercellular variability (CV: ~0.30) among the cells immediately preceding death (Figure 4F), with the intercellular variability staying robust from 20 to

0 generations before death. These observations indicate an approximately 2-fold increase in intercellular gene expression variability between young and old cell populations (Figures 4E and 4F). Interestingly, we saw that intercellular variability declines in the oldest cells aligned at birth (Figure 4E). Although this finding suggests that long-living cells can differentially resist the cause of mortality associated with changes in gene expression, the mechanistic connection between single-cell lifespan and intercellular gene expression variability is not fully understood.

We recently reported that haploid cells expressing YFP under the *GAL1* promoter exhibit reduced intracellular variability as they age (Liu et al., 2017). We asked whether the same phenomenon would be seen in diploid cells expressing a short-lived protein under a constitutive promoter. We investigated intracellular variability using a window of 8 generations to minimize the impact of random variation, and for consistency with our prior publication (Liu et al., 2017). Distinct from the intracellular noise reduction trend displayed by haploid cells, we observed that intracellular variability in diploid yeast remains relatively stable as cells age (Figure 4G), but increases shortly before death (Figure 4H), similar to our findings in haploid yeast (Liu et al., 2017). This abrupt increase in intracellular variability suggests that both haploid and diploid cells have diminished control over gene expression shortly before death. We note that the highest levels of intracellular variability observed in diploids approximates the lowest levels observed in haploids. The absence of intracellular noise reduction in diploids may be caused by the combined effect of a variety of factors. For example, because of the difference in ploidy, the abundances of housekeeping proteins and cellular machineries are also different between haploid and diploid cells, and the higher abundance in diploid cells may well provide a buffer that reduces the observed variability. Moreover, the promoters and the integration loci are different in the diploid experiments compared with the haploid, and differences in transcription factor and chromatin dynamics may also contribute to the different intracellular noise dynamics we observed in diploid cells.

Computational Modeling Suggests an Explanation for Intracellular Noise Dynamics

Based on computational simulations, we have previously proposed that the reduced intracellular variability of P_{GAL1}-YFP expression in haploid yeast cells may be due to increased stochastic promoter state transition rates as the cells age (Liu et al., 2017). To examine the potential impact of such transition rate increases on constitutive promoters in diploid yeast cells, we adapted the stochastic model used in the previous report for this study and fitted the resulting model to the experimentally measured fluorescence distribution to extract the value of model parameters (Tables S2–S4). We then varied the stochastic transition rates between ON and OFF states by up to 10-fold each in both directions and computed the resulting expression level and intracellular variability levels. We found that simultaneous increases in the OFF-to-ON transition rate (r_{ON}) and the ON-to-OFF transition rate (r_{OFF}) of the kind we previously postulated (indicated by the dashed line) left the level of intracellular expression variability largely unchanged under the parameter values used for these simulations (Figure S2). This suggests that the P_{TEF1} promoter operates at sufficiently high stochastic transition rates and that there is little potential for additional noise reduction. This is borne out by a comparison of the parameter values we extracted for the P_{TEF1} promoter (Table S4) with those we previously obtained for the P_{GAL1} promoter (Liu et al., 2017). It is also consistent with the fact that the diploid strains showed considerably less variation in expression level than the haploid P_{GAL1}-YFP strain we used previously (Figure S7), supporting our hypothesis that the diploid strains are at the "noise floor" with little room for further reduction.

Generality of Findings for Age-dependent Gene Expression and Noise Dynamics

The observations of gene expression dynamics described above are limited to a single genomic locus (*SAM2*), promoter (P_{TEF1}), and copy number (1, heterozygous). We next asked whether the phenotypes of protein concentration, abundance, and inter/intracellular noise described above were specific to the combination of factors investigated or global. For this purpose, we repeated the measurements made above for strains homozygous for P_{TEF1}-ssGFP at the *SAM2* locus (Figure 5), homozygous for P_{TEF1}-ssGFP at the *HIS3* locus (Figure 6), and homozygous for P_{PGK1}-ssGFP at the *HIS3* locus (Figure 7). Similar trends were found in all cases, indicating that the phenotypes described above are generalizable to constitutively expressed proteins with a half-life that approximates that of a typical, natural protein in yeast. Applying our stochastic model to the experimental data from these strains also yielded similar results (Figures S3, S4, and S6; Tables S5 and S7).

Protein Half-Life Drives Distinct Age-Related Expression Dynamics

A previous study in haploid cells demonstrated an age-related increase in long-lived fluorescent proteins expressed under the P_{TEF1} promoter (Zhang et al., 2012). We sought to replicate these results in our system

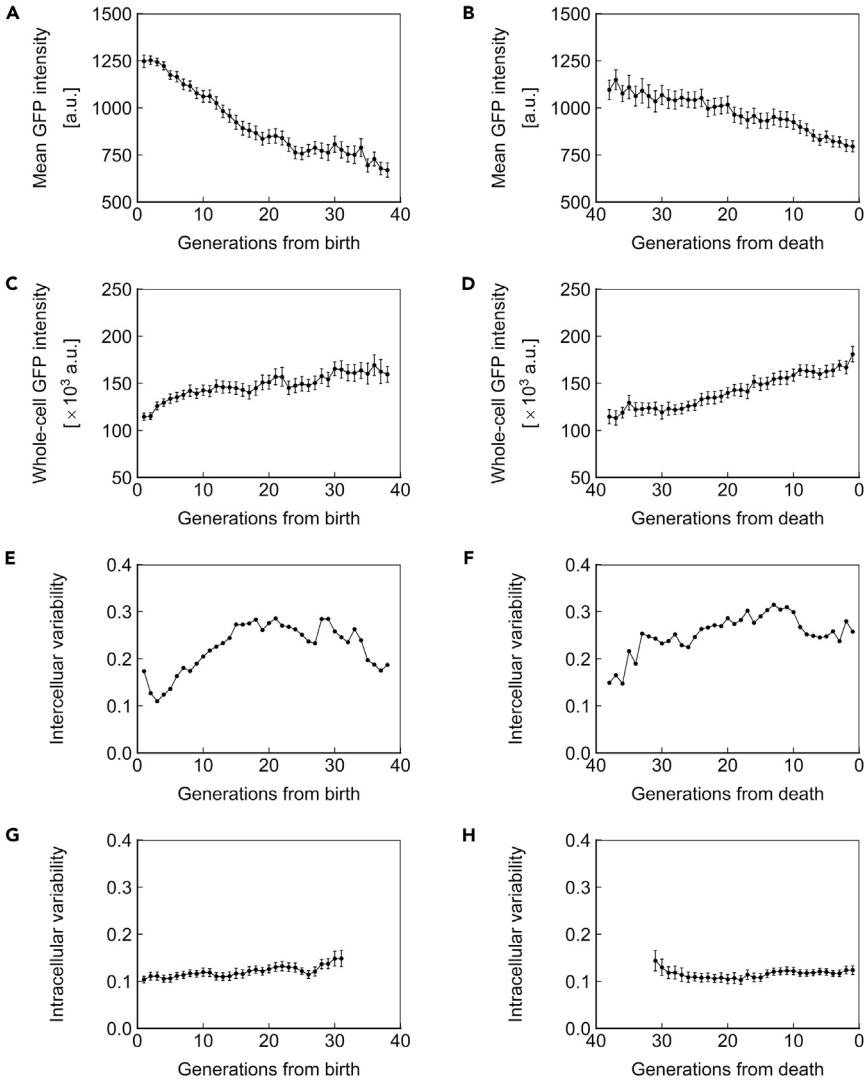

Figure 5. Dynamics of Homozygous P_{TEF1}-ssGFP at the *SAM2* Locus

(A and B) Mean ssGFP intensity, a measure of protein concentration, over generations for cells aligned to birth (A) or death (B).

(C and D) Whole-cell ssGFP intensity, a measure of protein abundance, over generations for cells aligned to birth (C) or death (D).

(E and F) Intercellular variability, defined as the SD divided by the mean of mean ssGFP intensity across measurements of all cells in the population at each generation. In (E), cells are aligned at birth, and in (F), cells are aligned at death.

(G and H) Mean intracellular variability, defined as the SD/mean of mean ssGFP intensity for 8 contiguous generations, over generations for cells aligned to birth (G) or death (H). All data represent measurements from a single experiment with ssGFP integrated in a homozygous fashion at the *SAM2* locus under the P_{TEF1} promoter. N = 50 cells for all subfigures, with data points where less than 10 cells remained alive omitted. Error bars are SEM.

See also Figures S3 and S7, and Tables S2–S4.

using a strain homozygous for P_{TEF1}-EGFP at the *HIS3* locus (Figures 8 and S5; Table S6). No change was detected in EGFP concentration for cells aligned to birth (Figure 8A). This result was surprising, given that a clear decline in ssGFP concentration was detected under identical circumstances (Figures 4A and 6A). Interestingly, a rapid increase in concentration was observed immediately before death (Figure 8B), inversely mirroring the decline observed for ssGFP (Figures 4B and 6B). We note that these results indicating stability of long-living fluorophore concentration during aging are consistent with results we obtained for P_{GAL1}-YFP in haploid yeast cells, including the observation of a rapid increase in concentration immediately before death.

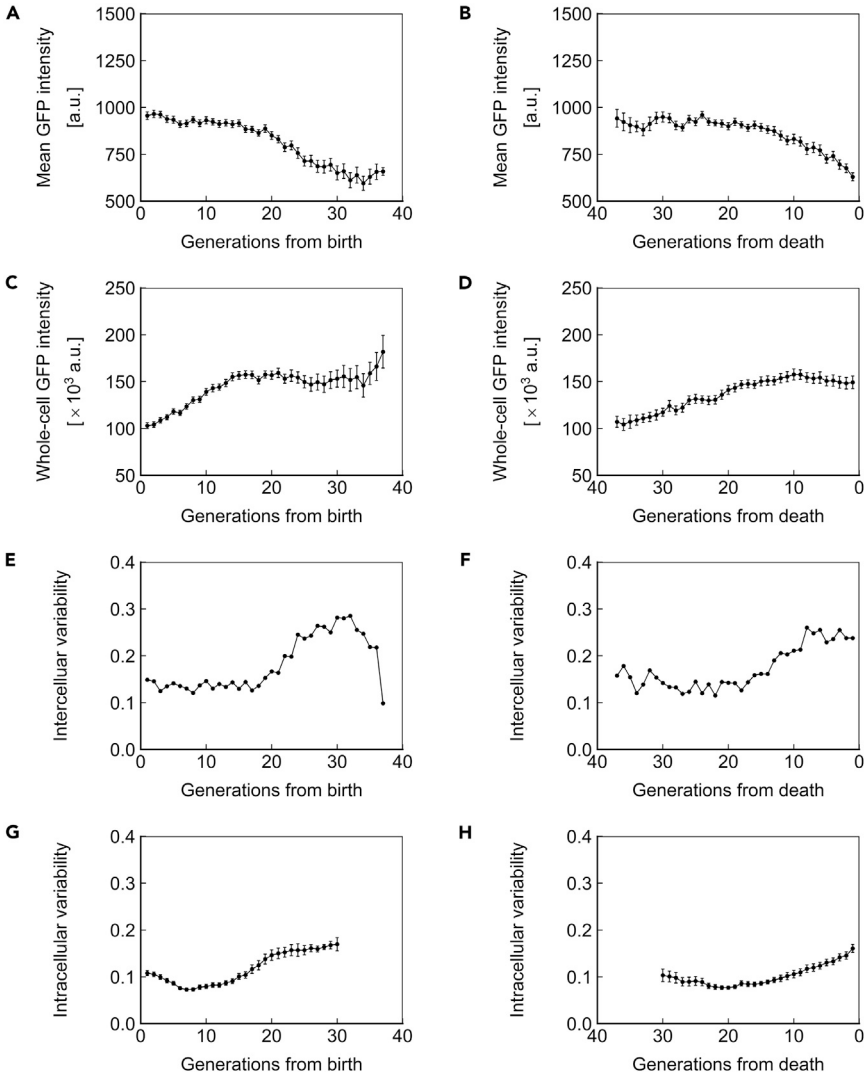

Figure 6. Dynamics of Homozygous P_{TEF1}-ssGFP at the *HIS3* Locus

(A and B) Mean ssGFP intensity, a measure of protein concentration, over generations for cells aligned to birth (A) or death (B).

(C and D) Whole-cell ssGFP intensity, a measure of protein abundance, over generations for cells aligned to birth (C) or death (D).

(E and F) Intercellular variability, defined as the SD divided by the mean of mean ssGFP intensity across measurements of all cells in the population at each generation. In (E), cells are aligned at birth, and in (F), cells are aligned at death.

(G and H) Mean intracellular variability, defined as the SD/mean of mean ssGFP intensity for 8 contiguous generations, over generations for cells aligned to birth (G) or death (H). All data represent measurements from a single experiment with ssGFP integrated in a homozygous fashion at the *HIS3* locus under the P_{TEF1} promoter. N = 50 cells for all subfigures, with data points where less than 10 cells remained alive omitted. Error bars are SEM.

See also Figures S4 and S7, and Tables S2, S3, and S5.

DISCUSSION

In this study, using a microfluidic device design optimized for the longitudinal tracking of diploid yeast cells, we present how a set of canonical cellular phenotypes dynamically change during the replicative aging of diploid yeast. A previous article from our laboratory provided insights into the dynamics of cell-intrinsic noise during the replicative aging of haploid yeast cells; using a stable fluorescent reporter (YFP) driven by the *GAL1* promoter integrated in the *ho* locus, single-cell YFP concentration and cell-intrinsic (intracellular) noise have been measured and reported. In the current study, we introduce a new

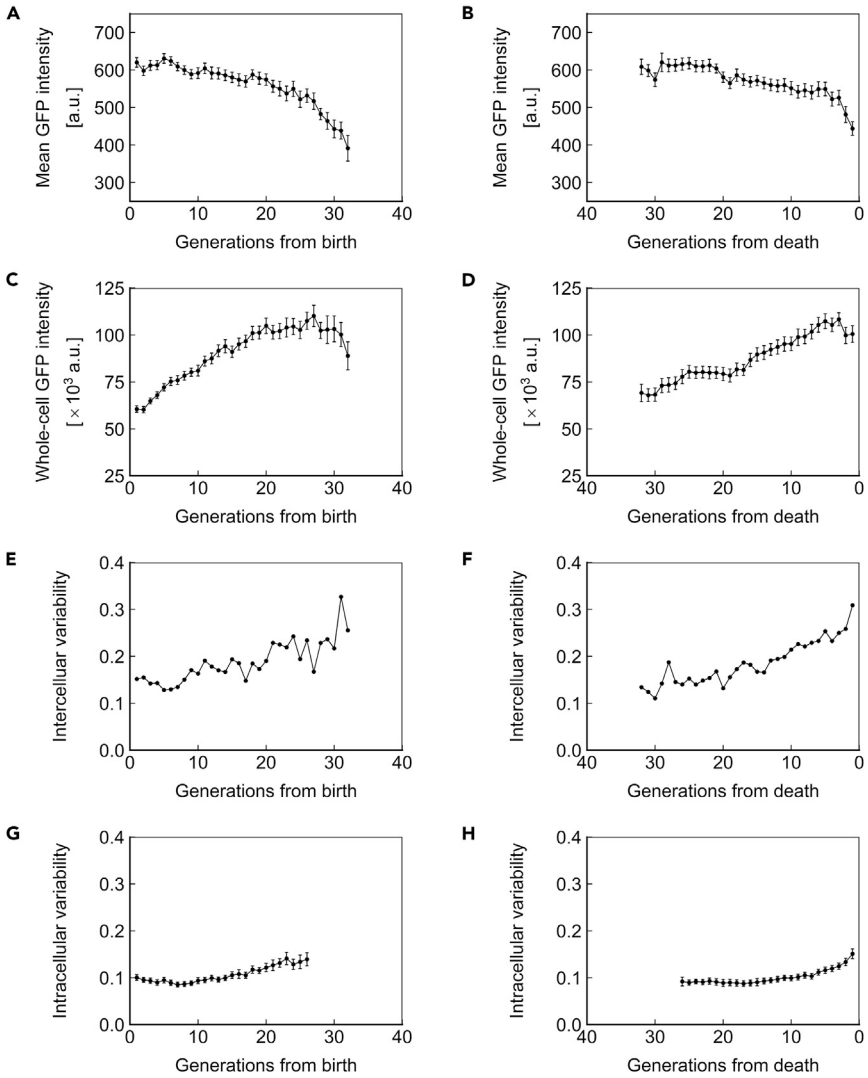

Figure 7. Dynamics of Homozygous P_{PGK1}-ssGFP at the *HIS3* Locus

(A and B) Mean ssGFP intensity, a measure of protein concentration, over generations for cells aligned to birth (A) or death (B).

(C and D) Whole-cell ssGFP intensity, a measure of protein abundance, over generations for cells aligned to birth (C) or death (D).

(E and F) Intercellular variability, defined as the SD divided by the mean for mean ssGFP intensity across measurements of all cells in the population at each generation. In (E), cells are aligned at birth, and in (F), cells are aligned at death.

(G and H) Mean intracellular variability, defined as the SD/mean of mean ssGFP intensity for 8 contiguous generations, over generations for cells aligned to birth (G) or death (H). All data represent measurements from a single experiment with ssGFP integrated in a homozygous fashion at the *HIS3* locus under the P_{PGK1} promoter. N = 50 cells for all subfigures, with data points where less than 10 cells remained alive omitted. Error bars are SEM.

See also Figures S6 and S7, and Tables S2, S3, and S7.

microfluidic device that can trap and track diploid yeast cells during replicative aging. Then, we directly show in aging mother cells that LOH is a rare event. We next elucidate the single-cell level dynamics of a wide variety of phenotypes during replicative aging: cell volume, cell division times, gene expression (in terms of both protein concentration and abundance), intracellular noise, and intercellular noise, with most of these characterizations performed using both stable and semi-stable reporter proteins driven by multiple promoters integrated at multiple loci. Finally, we use a stochastic model to gather quantitative mechanistic insights into the observed noise dynamics, which sheds light on the age-dependent intracellular noise differences between diploid and haploid yeast.

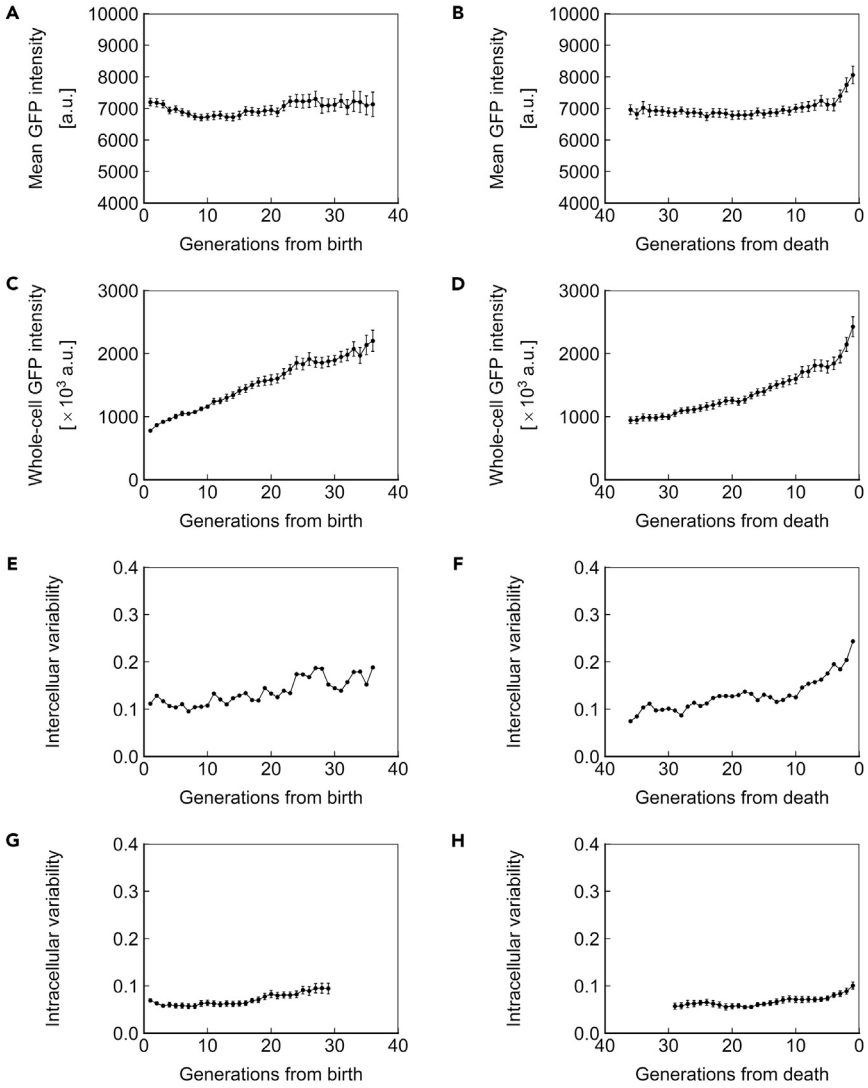

Figure 8. Dynamics of Homozygous P_{TEF1}-EGFP at the *HIS3* Locus

(A and B) Mean EGFP intensity, a measure of protein concentration, over generations for cells aligned to birth (A) or death (B).

(C and D) Whole-cell EGFP intensity, a measure of protein abundance, over generations for cells aligned to birth (C) or death (D).

(E and F) Intercellular variability, defined as the SD divided by the mean for mean EGFP intensity across measurements of all cells in the population at each generation. In (E), cells are aligned at birth, and in (F), cells are aligned at death.

(G and H) Mean intracellular variability, defined as the SD/mean of mean EGFP intensity for 8 contiguous generations, over generations for cells aligned to birth (G) or death (H). All data represent measurements from a single experiment with EGFP integrated in a homozygous fashion at the *HIS3* locus under the P_{TEF1} promoter. N = 50 cells for all subfigures, with data points where less than 10 cells remained alive omitted. Error bars are SEM.

See also Figures S5 and S7, and Tables S2, S3, S5, and S6.

The Duplicator enables the collection of single-cell microscopy data for hundreds of diploid *S. cerevisiae* cells throughout their full RLS. We used this technology to measure fundamental phenotypic characteristics associated with single-cell aging that were previously refractory to direct longitudinal investigation in a diploid genetic background. Our observations reveal new insights into the properties of cells during aging and near the end of life.

Consistent with our previous observations in haploids (Liu and Acar, 2018; Liu et al., 2017), the cell division times increased near the end of life in diploid yeast. This differs from observations for some other

unicellular organisms (Coelho et al., 2013; Wang et al., 2010). For instance, the fission yeast, *Schizosaccharomyces pombe*, does not exhibit increased cell division times before death when grown under favorable conditions (Coelho et al., 2013; Spivey et al., 2017). Similarly, the bacteria *Escherichia coli*, when grown in a microfluidic device, may undergo hundreds of divisions at an approximately constant rate before death (Wang et al., 2010). For both of these symmetrically dividing species, however, age-dependent division time differences have been observed under more stressful conditions (Rang et al., 2011; Stewart et al., 2005). Although information about the full spectrum of aging factors is limited, the difference in the age-dependent division time dynamics under stress-free conditions between these two species and *S. cerevisiae* may be due to the difference in their cell division styles. In contrast to *S. pombe* and *E. coli*, *S. cerevisiae* mother cell divides asymmetrically and produces a daughter cell that is significantly smaller than the mother. Assuming that certain aging factors are freely diffusible between mother and daughter compartments during cell division, the *S. cerevisiae* mother cell would be expected to have a diminished capability to dilute away aging factors through cell division compared with *S. pombe* and *E. coli*. If the impact of aging factors on *S. cerevisiae* division times is non-linear, the increased cell division times we observe near death could be interpreted as a reflection of the specific form of the non-linearity.

We also observed distinct age-related concentration dynamics for short-lived and long-lived proteins. A short-lived protein declined in concentration with age, whereas the concentration of a long-lived protein remained relatively stable. Protein concentration is a function of production and elimination. Since production of both proteins was controlled by the same promoter, the observed differences in concentration are the result of elimination. Protein elimination occurs due to both degradation and dilution by cell division. For long-lived proteins, dilution is the primary determinant of elimination, whereas degradation is the greater contributor to elimination for short-lived proteins. Dilution is driven by growth in cell volume, which proceeds at a constant rate until very late in life. Our observations therefore suggest an age-related increase in protein degradation rate. However, this would be unexpected, given that rapid degradation conferred by the CLN2PEST used in ssGFP is thought to be proteasome mediated (Schneider et al., 1998), and proteasome function has been suggested to decline with age (Andersson et al., 2013). One alternative explanation is that protein folding rates are reduced with age, and these effects are more obvious in ssGFP because maturation already takes a substantial portion of its lifetime.

The observation that protein half-life drives distinct age-related dynamics may be important in the context of gene networks. Many subcellular systems rely on a stoichiometric balance between their components (Birchler and Veitia, 2012; Kim and Forger, 2012). If two components experience distinct expression pressures arising from differences in half-life, a negative feedback mechanism would be essential to buffer the impact of the diverging expression pressures and prevent imbalance in the network. More specifically, the negative feedback would act by increasing the expression of the short-living protein in the network in response to age-related decreases in protein level, whereas it would decrease the expression of the long-living protein. We therefore hypothesize that gene networks have evolved to match the half-life of their components or finely control their stoichiometry via negative feedback, or that these age-related dynamics dependent upon protein half-life play a role in the aging process.

We found that protein abundance increased throughout the lifespan for both short- and long-lived proteins. For much of a cell's life, this increase in expression appears to compensate for the growth of cell volume to maintain protein concentration. However, abundance reaches a maximum at 5–10 generations before death, whereas volume continues to linearly increase. This closely matches the point at which the concentration of short-lived protein declines. These results suggest that some physical constraint on expression is reached several generations before cell death. Although there are numerous possibilities, the constraint could, for example, be facilitated by age-related damage experienced by the components of the gene expression machinery. In the case of long-lived proteins, for which concentration does not decline late in life, this leveling off of expression may be matched by a decrease in the rate of dilution, as cell cycle slows down in the last several generations of life.

Since cell volume increases linearly with age, the ratio of the abundance and concentration of a protein cannot remain constant during aging. Therefore, if both of these variables are optimized in young cells, they must necessarily diverge from their optimal values as the cell ages. Both the concentration and abundance of a protein might be relevant to biological function. For example, whereas concentration determines the rate of enzymatic reactions on a cell-wide scale, abundance could actuate compartmentalized activity in response to localization

cues. Since both concentration and abundance cannot remain constant, we envision that a protein with activities reliant on both would deviate from optimal function with age. We predict that either cells have evolved mechanisms to avoid this conundrum or that it plays a role in the process of aging.

Limitations of the Study

Our study here is limited to the behavior of an array of constitutive promoters during aging. Thus, it is possible that an inducible promoter may display different expression and noise dynamics during the aging process. The need to avoid phototoxicity during a multi-day aging study also places a limit on the achievable time resolution of expression level observations. Finally, our computational model does not attempt to model the effects of aging directly; instead, we examine the effect of parameter changes in the model to determine which parameters aging could have affected, which is necessarily indirect. Many model parameter values are also nearly impossible to measure directly and are obtained by estimation instead.

METHODS

All methods can be found in the accompanying Transparent Methods supplemental file.

SUPPLEMENTAL INFORMATION

Supplemental Information includes Transparent Methods, seven figures, seven tables, and one video and can be found with this article online at https://doi.org/10.1016/j.isci.2018.08.011.

ACKNOWLEDGMENTS

Facilities use was supported by the Yale Institute for Nanoscience and Quantum Engineering and NSF MRSEC DMR 1119826. The plasmid containing dsGFP, PTEF1-yEGFPCLN2PEST-pRS406 was a gift from Claudia Vickers (Addgene plasmid # 64406). E.A.S. acknowledges support through an NSF Graduate Research Fellowship and Gruber Science Fellowship. M.A. acknowledges funding through a New Scholar in Aging Award from the Ellison Medical Foundation (AG-NS-1015-13) and NIH Director's New Innovator Award (1DP2AG050461-01). We thank the Yale Center for Research Computing for guidance and use of the research computing infrastructure.

AUTHOR CONTRIBUTIONS

Conceptualization, E.A.S. and M.A.; Methodology, E.A.S., R.S., and M.A.; Software, R.S.; Formal Analysis, E.A.S. and R.S.; Investigation, E.A.S. and N.K.; Data Curation, E.A.S. and E.E.; Writing, E.A.S., R.S., and M.A.; Visualization, E.A.S. and R.S.; Supervision, E.A.S. and M.A.; Funding Acquisition, M.A.

DECLARATION OF INTERESTS

The authors declare no competing interests.

Received: July 20, 2018
Revised: August 1, 2018
Accepted: August 10, 2018
Published: September 28, 2018

REFERENCES

Andersson, V., Hanzén, S., Liu, B., Molin, M., and Nyström, T. (2013). Enhancing protein disaggregation restores proteasome activity in aged cells. Aging (Albany NY) *5*, 802–812.

Belle, A., Tanay, A., Bitincka, L., Shamir, R., and O'Shea, E.K. (2006). Quantification of protein half-lives in the budding yeast proteome. Proc. Natl. Acad. Sci. USA *103*, 13004–13009.

Birchler, J.A., and Veitia, R.A. (2012). Gene balance hypothesis: connecting issues of dosage sensitivity across biological disciplines. Proc. Natl. Acad. Sci. USA *109*, 14746–14753.

Chen, K.L., Crane, M.M., and Kaeberlein, M. (2017). Microfluidic Technologies for Yeast Replicative Lifespan Studies (Elsevier).

Coelho, M., Dereli, A., Haese, A., Kühn, S., Malinovska, L., DeSantis, M.E., Shorter, J., Alberti, S., Gross, T., and Tolić-Nørrelykke, I.M. (2013). Fission yeast does not age under favorable conditions, but does so after stress. Curr. Biol. *23*, 1844–1852.

Delaney, J.R., Chou, A., Olsen, B., Carr, D., Murakami, C., Ahmed, U., Sim, S., An, E.H., Castanza, A.S., Fletcher, M., et al. (2013). End-of-life cell cycle arrest contributes to stochasticity of yeast replicative aging. FEMS Yeast Res. *13*, 267–276.

Elowitz, M.B., Levine, A.J., Siggia, E.D., and Swain, P.S. (2002). Stochastic gene expression in a single cell. Science *297*, 1183–1186.

Ferrezuelo, F., Colomina, N., Palmisano, A., Garí, E., Gallego, C., Csikász-Nagy, A., and Aldea, M. (2012). The critical size is set at a single-cell level by growth rate to attain homeostasis and adaptation. Nat. Commun. *3*, 1012.

Herskowitz, I. (1988). Life cycle of the budding yeast *Saccharomyces cerevisiae*. Microbiol. Rev. *52*, 536–553.

Kim, J.K., and Forger, D.B. (2012). A mechanism for robust circadian timekeeping via stoichiometric balance. Mol. Syst. Biol. *8*, 630.

Liu, P., and Acar, M. (2018). The generational scalability of single-cell replicative aging. Sci. Adv. *4*, eaao4666.

Liu, P., Young, T.Z., and Acar, M. (2015). Yeast replicator: a high-throughput multiplexed microfluidics platform for automated measurements of single-cell aging. Cell Rep. *13*, 634–644.

Liu, P., Song, R., Elison, G.L., Peng, W., and Acar, M. (2017). Noise reduction as an emergent property of single-cell aging. Nat. Commun. *8*, 680.

Mateus, C., and Avery, S.V. (2000). Destabilized green fluorescent protein for monitoring dynamic changes in yeast gene expression with flow cytometry. Yeast *16*, 1313–1323.

McMurray, M.A., and Gottschling, D.E. (2003). An age-induced switch to a hyper-recombinational state. Science *301*, 1908–1911.

Natarajan, A., Subramanian, S., and Srienc, F. (1998). Comparison of mutant forms of the green fluorescent protein as expression markers in Chinese hamster ovary (CHO) and *Saccharomyces cerevisiae* cells. J. Biotechnol. *62*, 29–45.

Rang, C.U., Peng, A.Y., and Chao, L. (2011). Temporal dynamics of bacterial aging and rejuvenation. Curr. Biol. *21*, 1813–1816.

Raser, J.M., and O'Shea, E.K. (2004). Control of stochasticity in eukaryotic gene expression. Science *304*, 1811–1814.

Salama, S.R., Hendricks, K.B., and Thorner, J. (1994). G1 cyclin degradation: the PEST motif of yeast Cln2 is necessary, but not sufficient, for rapid protein turnover. Mol. Cell. Biol. *14*, 7953–7966.

Schneider, B.L., Patton, E.E., Lanker, S., Mendenhall, M.D., Wittenberg, C., Futcher, B., and Tyers, M. (1998). Yeast G1 cyclins are unstable in G1 phase. Nature *395*, 86–89.

Siudeja, K., Nassari, S., Gervais, L., Skorski, P., Lameiras, S., Stolfa, D., Zande, M., Bernard, V., Frio, T.R., and Bardin, A.J. (2015). Frequent somatic mutation in adult intestinal stem cells drives neoplasia and genetic mosaicism during aging. Cell Stem Cell *17*, 663–674.

Spivey, E.C., Jones, S.K., Rybarski, J.R., Saifuddin, F.A., and Finkelstein, I.J. (2017). An aging-independent replicative lifespan in a symmetrically dividing eukaryote. Elife *6*, e20340.

Steffen, K.K., Kennedy, B.K., and Kaeberlein, M. (2009). Measuring replicative life span in the budding yeast. J. Vis. Exp. e1209.

Stewart, E.J., Madden, R., Paul, G., and Taddei, F. (2005). Aging and death in an organism that reproduces by morphologically symmetric division. PLoS Biol. *3*, e45.

Swain, P.S., Elowitz, M.B., and Siggia, E.D. (2002). Intrinsic and extrinsic contributions to stochasticity in gene expression. Proc. Natl. Acad. Sci. USA *99*, 12795–12800.

Wang, P., Robert, L., Pelletier, J., Dang, W.L., Taddei, F., Wright, A., and Jun, S. (2010). Robust growth of *Escherichia coli*. Curr. Biol. *20*, 1099–1103.

Wasko, B.M., and Kaeberlein, M. (2014). Yeast replicative aging: a paradigm for defining conserved longevity interventions. FEMS Yeast Res. *14*, 148–159.

Wiktor-Brown, D.M., Hendricks, C.A., Olipitz, W., and Engelward, B.P. (2006). Age-dependent accumulation of recombinant cells in the mouse pancreas revealed by in situ fluorescence imaging. Proc. Natl. Acad. Sci. USA *103*, 11862–11867.

Yang, J., Dungrawala, H., Hua, H., Manukyan, A., Abraham, L., Lane, W., Mead, H., Wright, J., and Schneider, B.L. (2011). Cell size and growth rate are major determinants of replicative lifespan. Cell Cycle *10*, 144–155.

Zadrag-Tecza, R., Kwolek-Mirek, M., Bartosz, G., and Bilinski, T. (2009). Cell volume as a factor limiting the replicative lifespan of the yeast *Saccharomyces cerevisiae*. Biogerontology *10*, 481–488.

Zhang, Y., Luo, C., Zou, K., Xie, Z., Brandman, O., Ouyang, Q., and Li, H. (2012). Single cell analysis of yeast replicative aging using a new generation of microfluidic device. PLoS One *7*, e48275.

ISCI, Volume 7

Supplemental Information

Fundamental Characteristics of Single-Cell Aging in Diploid Yeast

Ethan A. Sarnoski, Ruijie Song, Ege Ertekin, Noelle Koonce, and Murat Acar

SUPPLEMENTAL FIGURES

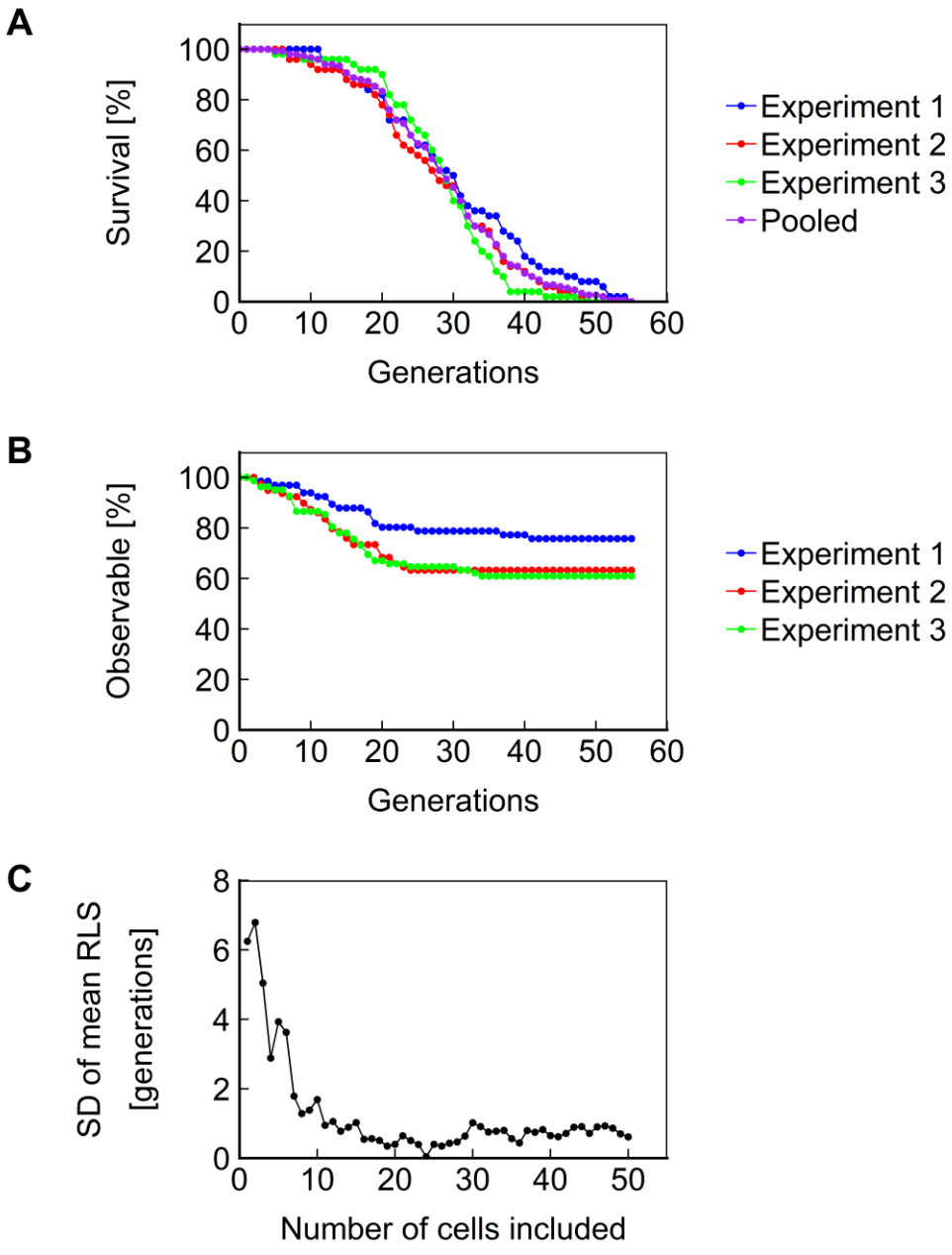

Figure S1. Validation of the Duplicator. Related to Figure 1. A. Survival curves of 50 cells each for three independent experiments performed using the wild-type BY4743 strain, and a pooled survival curve combining all 150 cells. **B.** Retention of cells in the experiments shown in (**A**), showing the fraction of cells that entered a trap and budded at least once prior to the 12th hour of the experiment, and remained within the field-of-view until a given age. **C.** Standard deviation of mean replicative lifespan calculated as a function of the number of cells included in the calculation.

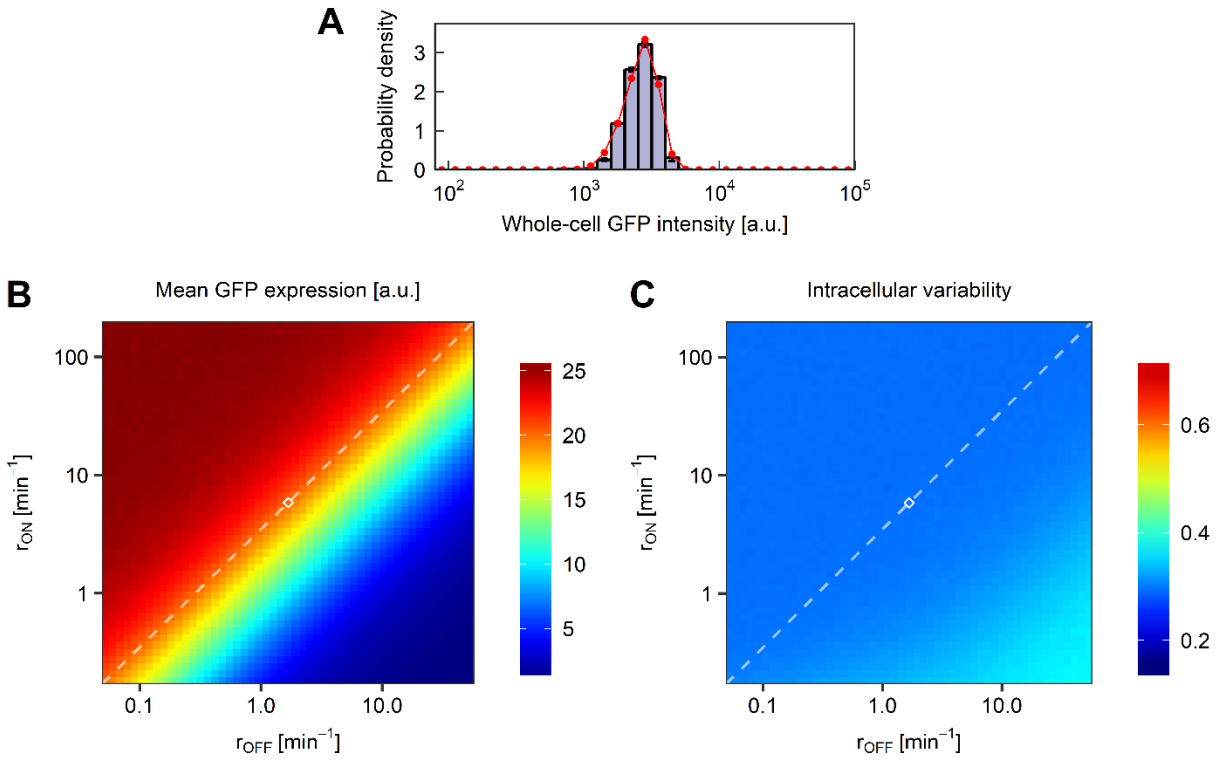

Figure S2. Model results for the heterozygous P_{TEF1}-ssGFP at *SAM2* locus strain. Related to Figure 4. **A.** Comparison of fit results (red) and experimental data for the heterozygous P_{TEF1}-ssGFP at *SAM2* locus strain. Error bars indicate s.e.m. (N=2). **B-C.** Effects of changes in r_{ON} and r_{OFF} on the mean expression level (**B**) and intracellular variability as measured by the coefficient of variation (**C**). White diamond indicates the fitted r_{ON} and r_{OFF} values. Dashed line indicates the result of simultaneous changes in r_{OFF} and r_{ON}.

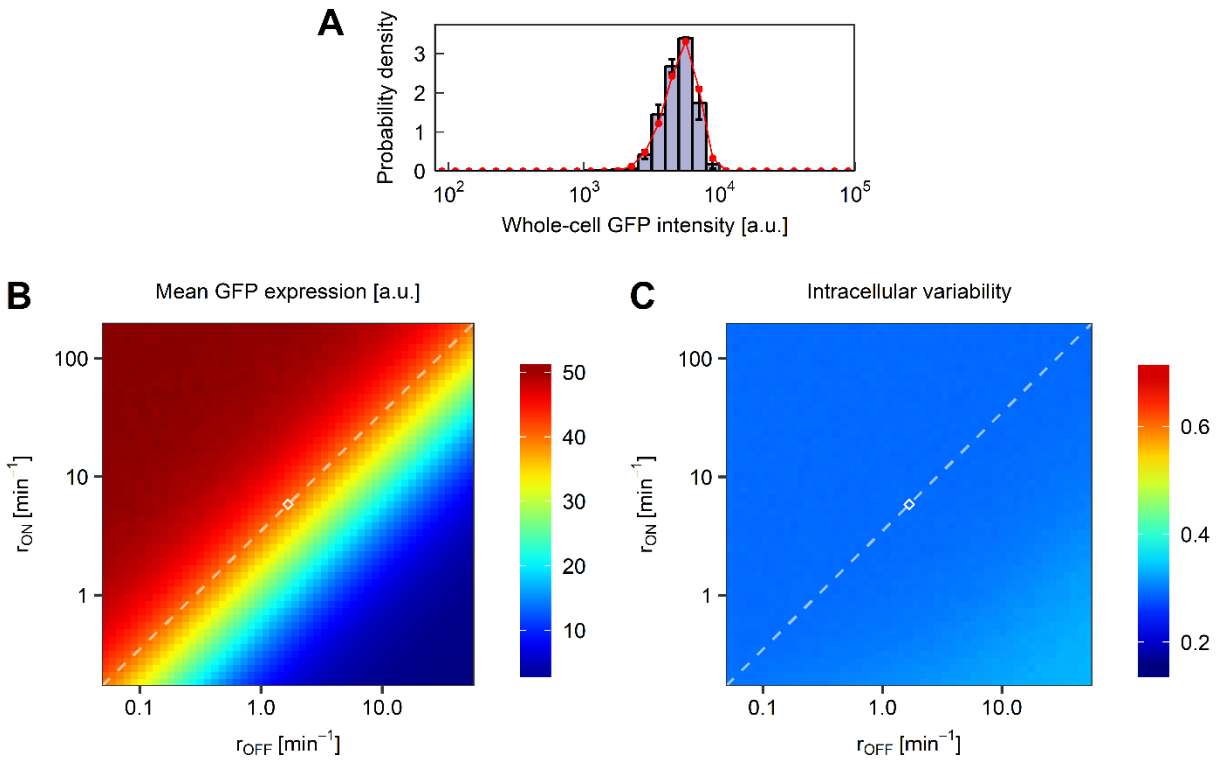

Figure S3. Model results for the homozygous P_{TEF1}-ssGFP at *SAM2* locus strain. Related to Figure 5. **A.** Comparison of simulation results (red) and experimental data for the homozygous P_{TEF1}-ssGFP at *SAM2* locus strain. Error bars indicate s.e.m. (N=2). **B-C.** Effects of changes in r_{ON} and r_{OFF} on the mean expression level (**B**) and intracellular variability as measured by the coefficient of variation (**C**). White diamond indicates the fitted r_{ON} and r_{OFF} values. Dashed line indicates the result of simultaneous changes in r_{OFF} and r_{ON}.

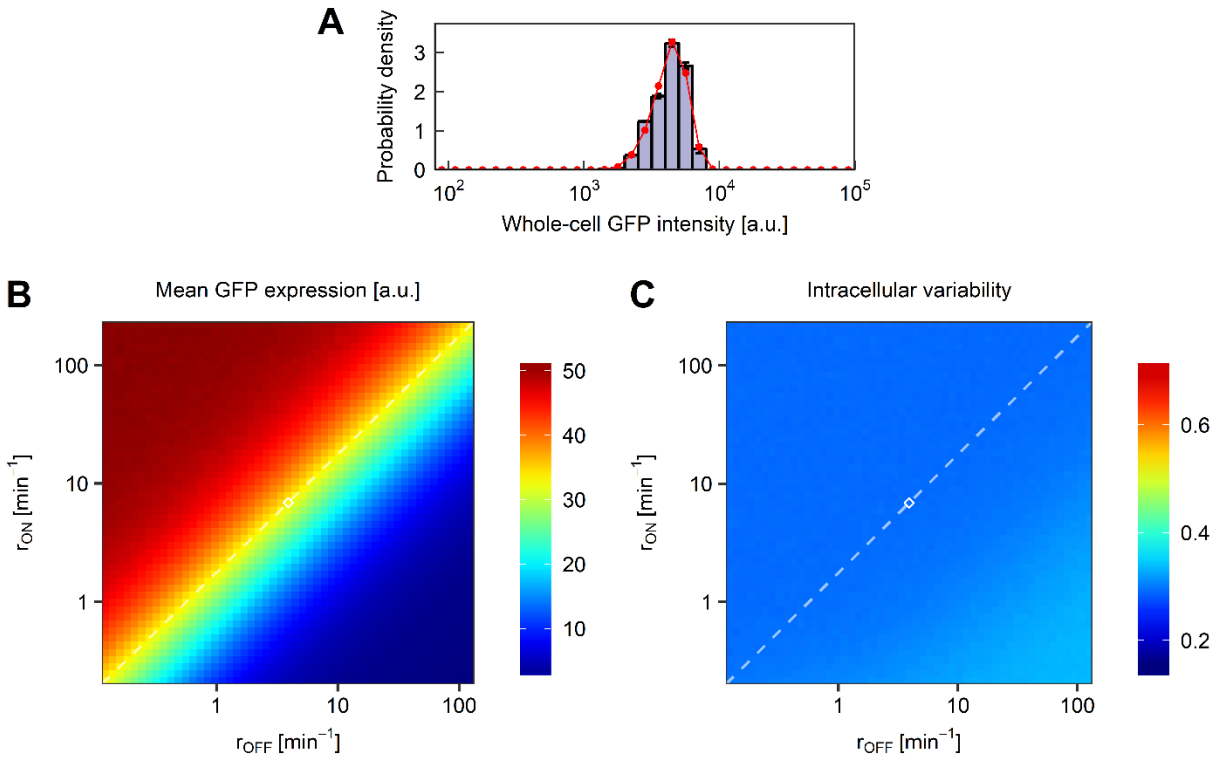

Figure S4. Model results for the homozygous P_{TEF1}-ssGFP at *HIS3* locus strain. Related to Figure 6. **A.** Comparison of fit results (red) and experimental data for the homozygous P_{TEF1}-ssGFP at *HIS3* locus strain. Error bars indicate s.e.m. (N=2). **B-C.** Effects of changes in r_{ON} and r_{OFF} on the mean expression level (**B**) and intracellular variability as measured by the coefficient of variation (**C**). White diamond indicates the fitted r_{ON} and r_{OFF} values. Dashed line indicates the result of simultaneous changes in r_{OFF} and r_{ON}.

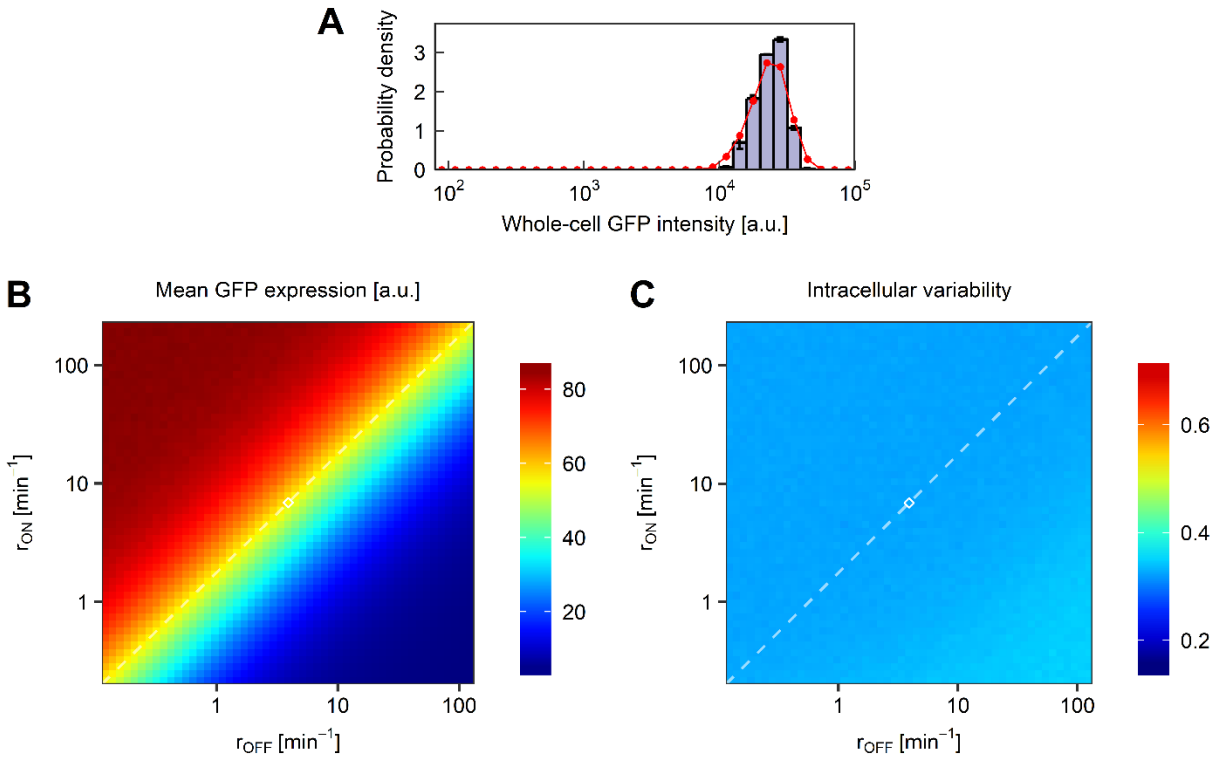

Figure S5. Model results for the homozygous P_{TEF1}-eGFP at *HIS3* locus strain. Related to Figure 8. **A.** Comparison of fit results (red) and experimental data for the homozygous P_{TEF1}-eGFP at *HIS3* locus strain. Error bars indicate s.e.m. (N=2). **B-C.** Effects of changes in r_{ON} and r_{OFF} on the mean expression level (**B**) and intracellular variability as measured by the coefficient of variation (**C**). White diamond indicates the fitted r_{ON} and r_{OFF} values. Dashed line indicates the result of simultaneous changes in r_{OFF} and r_{ON}.

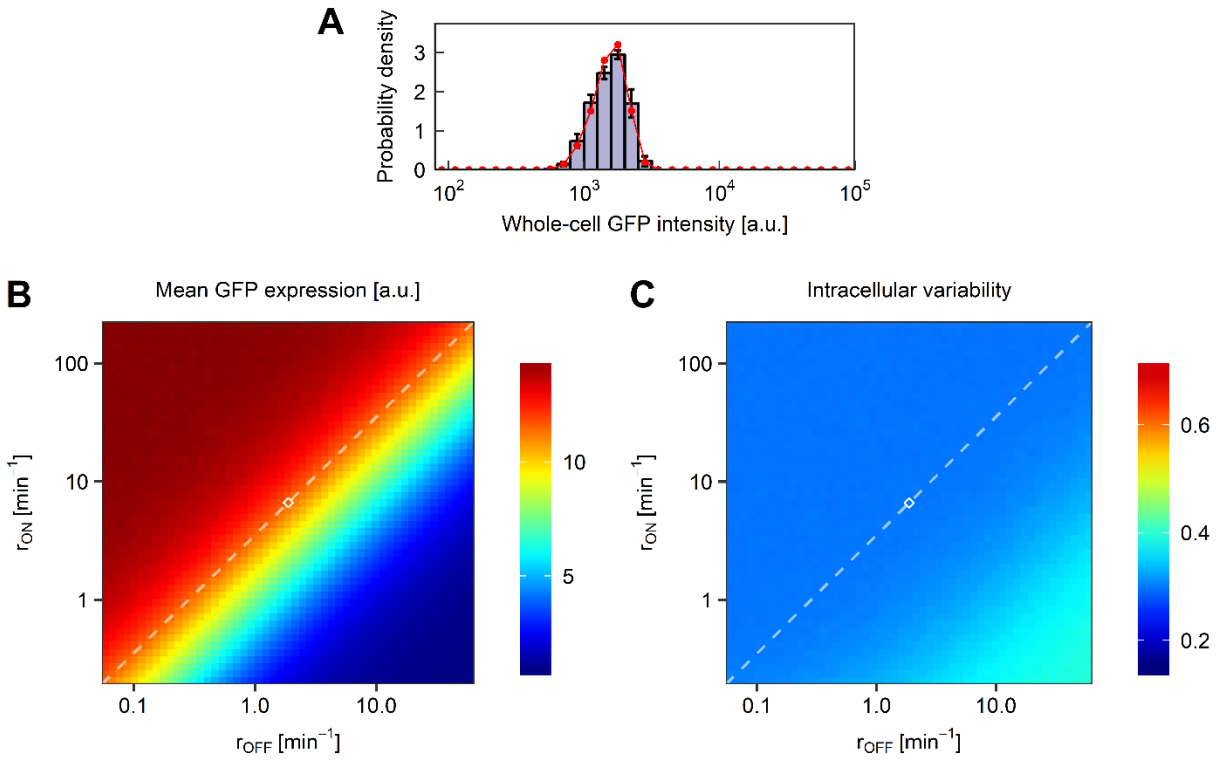

Figure S6. Model results for the homozygous P_{PGK1}-ssGFP at *HIS3* locus strain. Related to Figure 7. **A.** Comparison of fit results (red) and experimental data for the homozygous P_{PGK1}-ssGFP at *HIS3* locus strain. Error bars indicate s.e.m. (N=2). **B-C.** Effects of changes in r_{ON} and r_{OFF} on the mean expression level (**B**) and intracellular variability as measured by the coefficient of variation (**C**). White diamond indicates the fitted r_{ON} and r_{OFF} values. Dashed line indicates the result of simultaneous changes in r_{OFF} and r_{ON}.

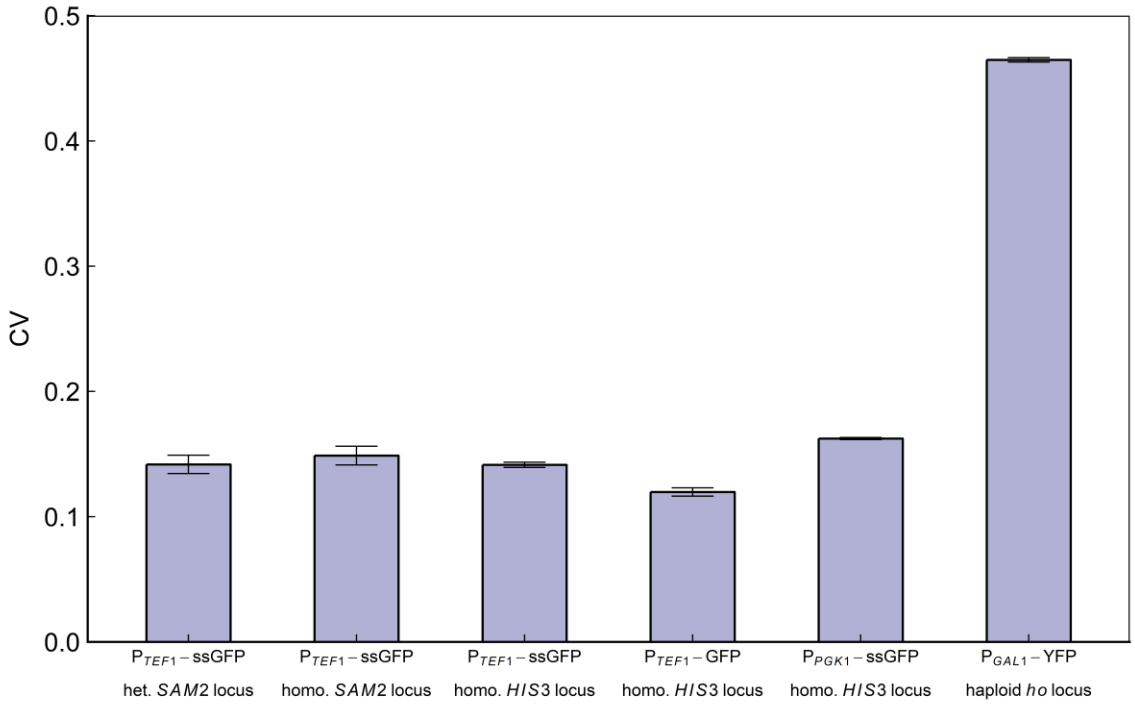

Figure S7. Comparison of population-level coefficients of variation between the five diploid strains under study and the P_{GAL1}-YFP haploid strain used in our previous work (Liu et al., 2017). Related to Figures 4-8. Error bars indicate s.e.m. (N=2).

SUPPLEMENTAL TABLES

Strain Description	Mean Lifespan
BY4743	30.44
BY4743	28.54
BY4743	28.06
BY4743 heterozygous for pTEF1-ssGFP at the SAM2 locus	28.51
BY4743 homozygous for pTEF1-ssGFP at the SAM2 locus	29.16
BY4743 homozygous for pTEF1-ssGFP at the HIS3 locus	29.46
BY4743 homozygous for pPGK1-ssGFP at the HIS3 locus	27.83
BY4743 homozygous for pTEF1-eGFP at the HIS3 locus	28.88

Table S1. Strains used and their mean lifespan characteristics. Related to Figure 1.

Parameter	Meaning	Value	Unit
mean and SD of r_1	Growth rate, G1	0.5 ± 0.125	fL min^{-1}
mean and SD of r_2	Growth rate, S/G2/M, total	1.5 ± 0.33	fL min^{-1}
mean and SD of r_{2m}	Growth rate, S/G2/M, mother compartment	0	fL min^{-1}
mean and SD of *T1'*	Minimum time before *start* for mothers	5 ± 2.5	min
mean and SD of *T2*	Time between *start* and S phase entry	5 ± 1.5	min
mean and SD of *T3*	Duration of S/G2/M	50 ± 5.78	min
mean and SD of V_i	Initial volume	75 ± 15	fL
k	Constants relating volume at *start* with r_1	160	min
b		24.0	fL
c	Level of inheritance for daughters	0.25	

Table S2. Parameters for the volume module. Related to Figures 4-8.

Parameter	Meaning	Value	Unit	References & Notes
r'_m	Apparent maximum transcription rate	2	min^{-1}	[Note A] [Note D]
r_p	Translation rate	1	min^{-1}	[Note A]
d_m	Degradation rate, mRNA	0.0346	min^{-1}	[Note A]
$d_{p,\ ssGFP}$	Degradation rate, ssGFP	0.00823	min^{-1}	[Note B]
$d_{p,\ eGFP}$	Degradation rate, eGFP	0.00101	min^{-1}	[Note B]
V_{ref}	Average volume of entire population	122	fL	[Note C]

Table S3. Fixed parameters for the gene network module. Related to Figures 4-8.

[Note A] Arbitrarily assigned. Any inaccuracy is accounted for during the fluorescence fitting process. To further improve generality, the additional initial conditions used (see Supplementary Text) have different values for these parameters.

[Note B] Calculated based on degradation data (Fig. 3).

[Note C] Assigned based on the results from running the volume model.

[Note D] Applicable to P_{TEF1} promoter in *SAM2* locus only. It is assumed that the actual transcription rate from the ON and OFF state promoter do not change with locus.

However, changes in the maximum fraction of time the promoter is in the ON state will lead to changes in the apparent maximum transcription rate (defined as the transcription rate measured at full induction).

Parameter	Meaning	Fitted value	Unit	Initial value	Lower bound	Upper bound
r_{ON}	Maximum OFF-to-ON transition rate	5.843	min^{-1}	1	0.01	10
f_{ON}	Fraction of time the promoter is in the ON state	0.7769		0.01	0.01	0.99
b'	Apparent basal expression level	0.0555		0.1	0	1
u_{ssGFP}	Fluorescence (a.u.) per ssGFP protein	0.6094		1	0.0001	10000
s	Volume noise scaling parameter	1.0424		0.25	0.01	2

Table S4. Fitted parameters for heterozygous P_{TEF1}-ssGFP in *SAM2* locus. Related to Figures 4 and 5.

Parameter	Meaning	Fitted value	Unit	Initial value	Lower bound	Upper bound
r_{ON}	Maximum OFF-to-ON transition rate	6.8803	min^{-1}	5.843	0.01	10
f_{ON}	Fraction of time the promoter is in the ON state	0.6379		0.7769	0.01	0.99

Table S5. Fitted parameters for homozygous P_{TEF1}-ssGFP in *HIS3* locus. Related to Figures 6 and 8.

Parameter	Meaning	Fitted value	Unit	Initial value	Lower bound	Upper bound
u_{eGFP}	Fluorescence (a.u.) per eGFP protein	1.88228		1	0.0001	10000

Table S6. Fitted parameters for homozygous P_{TEF1}-eGFP in *HIS3* locus. Related to Figure 8.

Parameter	Meaning	Fitted value	Unit	Initial value	Lower bound	Upper bound
r_{ON}	Maximum OFF-to-ON transition rate	6.6194	min^{-1}	5.843	0.01	10
f_{ON}	Fraction of time the promoter is in the ON state	0.7790		0.7769	0.01	0.99
b'	Apparent basal expression level	0.0793		0.0555	0	1
r'_m	Apparent maximum transcription rate	0.5710	min^{-1}	2	0.01	10

Table S7. Fitted parameters for homozygous P_{PGK1}-ssGFP in *HIS3* locus. Related to Figure 7.

TRANSPARENT METHODS

Yeast Strains, Media, and Culture Conditions

All experiments were conducted in a BY4743 strain background. Strains containing genetic modifications were constructed using lithium acetate transformation (Gietz and Schiestl, 2007). One or two copies of the specific [Promoter-Reporter-Terminator] cassettes were integrated in specific genomic loci in diploid yeast. Complete supplement mixture (CSM 2% glucose) was used as the media in all experiments. Media was prepared from powdered stock solutions fresh for each experiment. Cells were cultured in aerobic conditions and maintained at 30 °C in 50 mL conical tubes (Becton Dickinson F2070). All cultures were performed in an Innova-42 shaker (New Brunswick Scientific) at 225 rpm.

Design of the Duplicator

We aimed to create a device that would enable an automated microscope to image hundreds of diploid *S. cerevisiae* throughout the duration of their full RLS. A microfluidic channel containing structures designed to trap single cells is created between a soft plastic mold and a flat glass coverslip. Cells in culture media are introduced via an inlet and flow through the microfluidic channel into a waste container (Fig. 1A). Cells are tracked during aging by starting from their first generation; this is facilitated by having initially-loaded cells bud newborn daughters into the confines of a trap (Fig. 1B). Media is then flowed across the device for the duration of the experiment to wash daughter cells away and provide fresh nutrients. The Duplicator is mounted on an automated microscope, which images specified locations within the microfluidic chamber at regular intervals. This process generates a series of time-lapse images in which many cells can be observed from birth to death (Fig. 1C and Movie S1). The Duplicator was designed such that 16 separate channels could be affixed to a single 43 x 50 mm coverslip, each permitting observation of a different strain background or media condition.

Production of the Duplicator

The Duplicator is prepared by the joining of a glass coverslip and a PDMS cast prepared from a silicon wafer master mold. To prepare the mold, a silicon wafer with a 300 nm layer of thermal oxide (University Wafer #1583) was first coated in ZEP520A by spinning to equilibrium at 2000 rpm and baked at 180 °C for 5 minutes. The pattern of the microfluidic device was written into the resist with an electron beam lithography tool (EBPG, Raith), and developed by immersion in 0 °C xylenes for 20 seconds. The oxide layer was then etched using CHF_3 plasma in an Oxford Plasmalab 100 Reactive Ion Etching System. Next, the silicon was etched to a depth of 6 μm

using an Oxford Plasmalab 180 Reactive Ion Etching system set to cycle between SF_6 plasma and CHF_8 plasma. Finally, the remaining oxide was removed using CHF_3 plasma in the Oxford Plasmalab 100, and the wafer was washed thoroughly with water and dried with nitrogen gas.

To prepare the PDMS cast, the wafer mold was first placed into a small dish constructed of tight-fitting aluminum foil. This assembly was placed under vacuum adjacent to several drops of trichlorosilane (Sigma #448931) in a foil bowl for 20 minutes to vapor-coat the wafer. Afterward, a mixture of PDMS elastomer and curing agent (Dow Corning Sylgard 184 Silicone Elastomer Kit) was prepared in a 10:1 mass ratio totaling 44 g, and poured onto the surface of the wafer. The wafer was placed under vacuum for several hours until fully debubbled, and heated at 150 °C for 20 minutes to cure the PDMS. After cooling to room temperature, the PDMS was cut from the wafer with a sharp blade. Two inlet and one outlet holes were punched in each lane of the microfluidic device using a Schmidt Press (Syneo). The PDMS was thoroughly cleaned with isopropanol and dried. Finally, the PDMS was bonded to a clean 43 x 50 mm glass slide (Gold Seal #3329) using a corona treater (Electro-Technic Part 085-0057-3 BD-20ACV).

Performance validation for the Duplicator

Our first objective was to assess the reproducibility of results obtained from our device. We conducted three identical experiments in which we loaded cells to the device, and for 120 hours imaged 20 locations at 10-minute intervals. For each experiment, we assessed the lifespan of 50 wild-type cells (Fig. S1A). The mean$\pm$s.e.m. lifespan for cells from all three experiments was 29.0$\pm$0.7 generations, with mean values for each individual experiment falling within 5% of the overall mean value. This RLS approximates published values for the diploid BY4743 strain used in these experiments (Delaney et al., 2013; Yang et al., 2011).

In addition to lifespan, we investigated the retention rate of cells that became trapped in the device. For each of the experiments above, we noted the number of newborn cells that entered a trap, but escaped prior to their death. We found that 61% - 76% of the newborn cells that entered a trap and budded at least once could be observed for the duration of their lifespan (Fig. S1B). While this value is less than the 98% retention rate of the Replicator, we find that it is sufficient to measure lifespan for approximately 100 cells in each lane of the device (Fig. S1C). The retention rate of the Duplicator could be further increased by slightly decreasing the area of the trapping units in the device. However, we opted against it as such a decrease would hamper the precision of the measurements for cellular area and perimeter.

Duplicator Experiments

18” of tubing (Cole-Parmer 06419-00) was connected to the outlet and cell inlet of each Duplicator lane. 12” of the same tubing was connected to the media inlet. The media inlet was connected to a 250 mL flask (Duran 10-922-34) attached to a digital pressure regulator (Fluigent MFCS). Media was introduced to the device at a pressure of 100 mbar, and the cell inlet was stoppered with an insect pin. The traps within the channel were debonded from the glass slide by increasing pressures of up to 1900 mbar. Cells were cultured for 18 hours to an approximate OD_{600nm} of 0.7, and introduced via the cell inlet at a rate of 10 µL/minute using a syringe pump (New Era Pump Systems Inc., NE-1000) with media pressure set to 100 mbar. After loading, the cell inlet was backflushed with media at 130 mbar for 30 minutes to remove all cells from the inlet tubing, where their growth would create clogging in the microfluidic device. During the flush, an automated microscope was used to select 20 imaging locations within each lane of the microfluidic device. The right-most traps were avoided, as those too close to the outlet experienced a high rate of cell loss. After the flush, media pressure was set to 100 mbar, and the cell inlet tubing was clamped shut with a 1” binder clip. The automated microscope was set to image the device at regular intervals, typically of 10 minutes, for 120 hours. Media pressure was set to oscillate and increase over time to prevent clogging of the device as aged, enlarged cells became more prevalent in the population.

Measurements in the Duplicator Device

RLS was scored manually by observing the time-lapse image series produced in a Duplicator experiment. Cells were included for measurement if they completed at least one budding cycle while alone in the trap prior to the 12th hour of the experiment. Passage into each generation was denoted by the appearance of a bud. The results of all RLS measurements are shown in Supplementary Table S1. Fluorescence and area measurements were made using the Bezier circling tool of the NIS Elements Advanced Research software. Fluorescence measurements used for analysis and graphing were first subjected to background subtraction with the average GFP intensity for 10 wild-type cells throughout their lifespan.

Estimation of Cell Volume

The area and perimeter of cells was measured at hourly intervals, simultaneous to the measurement of fluorescence intensity. We assumed that diploid yeast could be approximated as ellipsoid. Therefore, cell volume is defined by the formula $Volume = \frac{4}{3}\pi a^2 b$ where a represents the radius along the short axis, and b is the radius of the long axis. Working from a 2-dimensional

image taken at the center of the ellipse, we set $a+b=\sqrt{2\frac{Perimeter^2}{2\pi}+\frac{Area}{\pi}}$ and $a-b=\sqrt{2\frac{Perimeter^2}{2\pi}-\frac{Area}{\pi}}$, then solved for a and b. In the rare instance that $a^2<b$, our equations were invalid. These data points were omitted.

Flow Cytometry

All measurements were performed using a BD FACSVerse, with cells grown for 18 hours to mid-log phase, an OD_{600} of 0.1-1, at the start of the experiment. For half-life measurements, cycloheximide (Sigma C4859) was added to each culture to a concentration of 10 µg/mL. The cultures were then returned to the shaking incubator, with aliquots taken every 10 minutes for flow cytometry. For other modeling measurements, cultures were placed on ice after 18 hours, then immediately used for flow cytometry.

Description of the Stochastic Model

We adapted our previously described stochastic model (Liu et al., 2017) to the expression of ssGFP and GFP from the TEF1 and PGK1 promoters. Briefly, the promoter is assumed to stochastically switch between two states, OFF and ON. Transcription occurs at the basal rate in the OFF state and at the maximal rate in the ON state. The resultant mRNA is translated to produce the fluorescent reporter, and both protein and mRNA can be degraded.

Volume and cell cycle is controlled by a separate volume module based on previous work (Ferrezuelo et al., 2012). The cell cycle is divided into two parts: G1 and S/G2/M, with the volume increasing linearly, but at different rates, in each part of the cell cycle. The G1 phase growth rate (an independent variable) is linearly related to the volume at which the cell enters S, with a separate floor on G1 phase duration so that mother cells do not immediately reenter S. We fixed the volume module parameters to be generally consistent with our experimental measurements (Fig. 2, Table S2). Protein degradation rates were fixed based on our measurements, and other parameters related to mRNA and protein synthesis and mRNA degradation were fixed from general ranges reported in literature (Table S3).

In each case, experimental data was obtained by flow cytometry. The model was fitted to the data using the same procedure as previously described (Liu et al., 2017). To summarize, a population of 25,000 freely dividing cells were simulated with resampling every 40 minutes to keep the population size approximately constant. At the end of the simulation, the reporter protein (ssGFP) level in each cell is converted to a simulated fluorescence level and a simulated

fluorescence distribution is obtained. The Nelder-Mead algorithm (Nelder and Mead, 1965), as implemented in the NLopt (Johnson, 2014) library, is used to find parameter values that maximize the likelihood of observing the experimental distribution.

To determine the effects of the promoter dynamics parameters r_{ON} and r_{OFF} on intracellular expression variability, we systematically varied each in a wide range (between 10% and 1000% of the fitted value). An initial population of 20,000 exponentially growing cells were simulated for 24 hours with periodic resampling to ensure that they have reached steady state, and then 5,000 cells were randomly sampled from the population and simulated for another 40 generations. In this second stage, only the 5,000 cells themselves are considered (daughters are discarded), and the reporter protein expression level in each cell is recorded every 10 minutes and used to calculate the intracellular variability level for each cell (expressed as the coefficient of variation). The calculated intracellular variability level for all 5000 cells are then averaged to produce an intracellular variability value for the entire population.

Heterozygous P_{TEF1}-ssGFP, *SAM2* locus

We determined the fitted parameter values for this strain and the conversion factor from ssGFP to simulated fluorescence by fitting the simulation output to the experimentally observed distribution (Table S4). The results are shown in Figure S2. Simultaneous changes in the values of r_{ON} and r_{OFF} as we previously postulated for P_{GAL1} in haploid cells (Liu et al., 2017) has minimal effects on the level of intracellular variability for this promoter.

Homozygous P_{TEF1}-ssGFP, *SAM2* locus

We performed simulations for the homozygous case by using the same fitted parameters for the heterozygous case, merely increasing the number of copies of the gene in the model from 1 to 2. The results are shown in Figure S3 and are extremely similar to the heterozygous strain after accounting for the roughly doubled level of expression.

Homozygous P_{TEF1}-ssGFP, *HIS3* locus

We fitted the promoter dynamics parameters of this strain to account for the different locus (Table S5), keeping all other parameters at the same value. The results are shown in Figure S4 and are also quite similar to the previous ones except for the expression level difference.

Homozygous P_{TEF1}-eGFP, *HIS3* locus

The degradation rate difference alone cannot explain the 5-fold difference in the experimentally observed mean fluorescence levels of the ssGFP and eGFP strains. We therefore postulated that

the additional tag may have also made ssGFP less bright than eGFP, and fitted the fluorescence conversion factor of eGFP for this strain (Table S6), keeping all other parameters at the same value. The results are shown in Figure S5 and are once again quite similar to the previous strains.

Homozygous P_{PGK1}-ssGFP, *HIS3* locus

We fitted the promoter dynamics and transcription parameters of this strain to account for the different promoter (Table S7), keeping all other parameters at the same value. The results are shown in Figure S6 and are also quite similar to the previous ones except for the expression level difference.

Different initial conditions

For each of these 5 strains, we also repeated the entire analysis for 9 additional sets of initial conditions. The results are not materially different: in all cases, the intracellular noise value is not substantially affected by increases in the promoter dynamics parameters, indicating that the two constitutive promoters under study are already at the "noise floor" such that the potential for additional noise reduction is minimal.

Different doubling times

Because the single-cell level doubling time was experimentally observed to vary over time as the cell ages, we further repeated the analysis for four separate doubling time values (80 minutes, 120 minutes, 160 minutes and 200 minutes) for all strains and initial conditions. We observed a minor decrease in intracellular variability levels from increasing the doubling time, which is due to increases in the reporter protein concentration (as expected due to reduced dilution).

Experimental observations are consistent with "noise floor"

We computed the population-level coefficients of variation of GFP fluorescence (as measured by flow cytometry) for all five strains and compared them to the CV calculated for the haploid *gal80Δ* strain carrying P_{GAL1}-YFP in *ho* locus. As can been seen from Figure S7, all five strains have substantially less intercellular variability than the haploid P_{GAL1}-YFP strain, with the CV values being roughly one-third of that strain. This corroborates our hypothesis that the five diploid strains are at the "noise floor" with little room for further reduction.

SUPPLEMENTAL REFERENCES

Gietz, R.D., and Schiestl, R.H. (2007). High-efficiency yeast transformation using the LiAc/SS carrier DNA/PEG method. Nat. Protoc. *2*, 31–34.

Johnson, S.G. (2014). The NLopt nonlinear-optimization package.

Nelder, J.A., and Mead, R. (1965). A Simplex Method for Function Minimization. Comput. J. *7*, 308–313.